universität wien

MASTERARBEIT | MASTER'S THESIS

Titel | Title

The Immunomodulatory Role of A20 in EGFR-Mutant Lung Adenocarcinoma

verfasst von | submitted by

Max Albert Schwab

angestrebter akademischer Grad | in partial fulfilment of the requirements for the degree of

Master of Science (MSc)

Wien | Vienna, 2025

Studienkennzahl lt. Studienblatt | Degree programme code as it appears on the student record sheet:	UA 066 865
Studienrichtung lt. Studienblatt | Degree programme as it appears on the student record sheet:	Masterstudium Molecular Biology
Betreut von | Supervisor:	Univ.-Prof. Dr. Emilio Casanova

Acknowledgements

I want to express my gratitude to Prof. Dr. Emilio Casanova for the opportunity of conducting my master's thesis in his lab and for his valuable expertise and feedback during lab meetings and discussions.

Furthermore, I want to thank Dr. Herwig Moll for supervising my project, always being open for discussions, planning experiments and providing valuable feedback.

Next, I would like to say special thanks to Monika Homolya, for mentoring me throughout my project and always making time for helping me, discussing experiments and results and guiding me through my research project.

Many thanks to Natalie Schindler for her support in the lab, during our thesis writing sessions in the library, and for always being up for much-needed coffee breaks.

Lastly, I want to give thanks to my colleagues and lab member Khushi Asnani, Maša Bereš, Faith David, Jaqueline Horvath, Eva Putz, Michael Machtinger, Christoph Trenk, Marija Trkulja, Sarah Trouvilliez for guidance, assistance, and the warm welcome I received in the group.

Abstract

Lung cancer is the leading cause of cancer-related deaths worldwide. Chronic inflammation is highly associated with lung tumorigenesis, particularly in lung adenocarcinoma (LUAD), the most common subtype of non-small cell lung cancer (NSCLC). Tumor necrosis factor alpha-induced protein 3 (TNFAIP3), commonly known as A20, is a negative feedback regulator of the pro-inflammatory nuclear factor kappa B (NF-κB pathway). A20 was recently shown to be a potent tumor suppressor in Kirsten rat sarcoma virus (KRAS)-mutant LUAD. Loss of A20, frequently observed in LUAD tumors, promotes immune escape and hence reduced survival in KRAS-mutant lung tumors, but also makes them more susceptible to anti-programmed cell death-ligand 1 (PD-L1) therapy. However, the role of A20 in epidermal growth factor receptor (EGFR)-mutant lung cancer, the second most common oncogenic driver in LUAD, remains unclear. This thesis investigates the functions of A20 in EGFR-driven LUAD tumorigenesis, to assess its potential as a prognostic marker for immunotherapy. By using genetically engineered mouse models, we demonstrate that tumor-intrinsic loss of A20 in immunogenic EGFR-mutant tumors leads to a reduced tumor burden and improved survival, opposite to the phenotype previously observed in KRAS-mutant LUAD. Given its known immunomodulatory potential, we investigated the impact of A20 in modulating tumor immune cell infiltration, revealing that A20-deficient tumors show an increase in T cell and decrease in macrophage infiltration 18 weeks post tumor initiation. Furthermore, RNA sequencing data revealed an upregulation of genes associated with T cell migration and activation in A20-deficient LUAD cells. Additionally, human EGFR-mutant LUAD cells exhibited increased signal transducer and activator of transcription 1 (STAT1) activation and reduced proliferation and sensitivity to the tyrosine kinase inhibitor (TKI) osimertinib upon loss of A20. These findings underscore the dual role of A20 in lung cancer as a tumor suppressor or oncogene, dependent on the oncogenic driver, and suggest that A20 activity may influence the efficacy of immunotherapy in EGFR-mutant LUAD.

Zusammenfassung

Lungenkrebs ist weltweit die häufigste Ursache für krebsbedingte Todesfälle. Chronische Entzündungen stehen in engem Zusammenhang mit der Tumorbildung in der Lunge, insbesondere beim bronchialen Adenokarzinom (LUAD), der häufigsten Art des nichtkleinzelligen Bronchialkarzinoms (NSCLC). Tumornekrosefaktor-alpha-induziertes Protein 3 (TNFAIP3), auch bekannt als A20, ist ein negativer Regulator des pro-inflammatorischen Nuklearfaktor-Kappa-B (NF-κB) Signalwegs. A20 erwies sich kürzlich als ein wirksamer Tumorsuppressor in Kirsten-Rat-Sarkom-Virus (KRAS)-mutiertem LUAD. Der Verlust von A20, der häufig bei LUAD-Tumoren beobachtet wird, begünstigt die Immunflucht und führt damit zu einer geringeren Überlebensrate bei KRAS-mutierten Lungentumoren, erhöht aber auch die Anfälligkeit für anti-programmierten Zelltod-Liganden 1 (PD-L1) Therapie. Die Rolle von A20 bei Lungenkrebs mit einer EGFR-Mutation (epidermaler Wachstumsfaktorrezeptor), dem zweithäufigsten onkogenen Treiber bei LUAD, bleibt jedoch unklar. In dieser Arbeit werden die Funktionen von A20 in der EGFR-getriebenen LUAD-Tumorgenese untersucht, um sein Potenzial als prognostischen Marker für die Immuntherapie zu bewerten. Anhand von genetisch modifizierten Mausmodellen zeigen wir, dass der tumorintrinsische Verlust von A20 in immunogenen EGFR-mutierten Tumoren zu einer geringeren Tumorlast und einer verbesserten Überlebensrate führt, dem entgegengesetzten Phänotyp, der zuvor bei KRAS-mutierten LUAD beobachtet wurde. Angesichts des bekannten immunmodulatorischen Potenzials von A20 untersuchten wir die Auswirkungen von A20 auf die Infiltration von Immunzellen in Tumoren und stellten fest, dass A20-defiziente Tumoren 18 Wochen nach Tumorinitiation eine Zunahme der T-Zell- und eine Abnahme der Makrophageninfiltration aufweisen. Außerdem zeigten RNA-Sequenzierungsdaten eine Hochregulierung von Genen in A20-defizienten LUAD, die mit der T-Zell-Aktivität in Verbindung stehen. Zusätzlich zeigten humane EGFR-mutierte LUAD-Zellen eine verstärkte Aktivierung des Signaltransduktors und Transkriptionsaktivators 1 (STAT1) sowie eine verringerte Proliferation und Sensitivität gegenüber dem Tyrosinkinasehemmer (TKI) Osimertinib nach A20-Verlust. Diese Ergebnisse betonen die Doppelfunktion von A20 bei Lungenkrebs als Tumorsuppressor oder Onkogen, abhängig vom onkogenen Treiber, und legen nahe, dass die A20-Aktivität die Wirksamkeit der Immuntherapie bei EGFR-mutiertem LUAD beeinflussen könnte.

Table of Contents

List of Abbreviations

ABC	ATP-binding cassette
AKT	AKT serine/threonine Kinase 1
ALK	Anaplastic lymphoma kinase
ANOVA	Analysis of Variance
APEX1	Apurinic/Apyrimidinic endodeoxyribonuclease 1
ATM	ATM serine/threonine kinase
ATP	Adenosine triphosphate
BRAF	V-raf murine sarcoma viral oncogene homolog b1
BTC	Betacellulin
CD	Cluster of differentiation
CDKN2A	Cyclin dependent kinase inhibitor 2A
CMV	Cytomegalovirus
CRISPR	Clustered regularly interspaced short palindromic repeats
CTLA-4	Cytotoxic T-lymphocyte–associated antigen 4
CXCL	C-X-C motif chemokine ligand
CXCR	C-X-C Motif chemokine receptor
DNA	Deoxyribonucleic acid
DOX	Doxycycline
EGF	Epidermal growth factor
EGFR	Epidermal growth factor receptor
EMT	Epithelial-mesenchymal transition
ERK	Extracellular signal-regulated kinase
FDA	U.S. Food and Drug Administration
GAP	GTPase-activating proteins
GDP	Guanosine diphosphate
GEF	Guanine nucleotide exchange factors

GRB2	Growth factor receptor-bound protein 2
GSEA	Gene set enrichment analysis
GTP	Guanosine triphosphate
HBEGF	Heparin-binding EGF-like growth factor
HDAC3	Histone deacetylase 3
HER	Human epidermal growth factor receptor
HSP70	Heat shock protein 70
IC50	Half-maximal inhibitory concentration
ICAM	Intercellular adhesion molecule 1
ICB	Immune checkpoint blockade
ICI	Immune checkpoint inhibitor
IFN-γ	Interferon gamma
IHC	Immunohistochemistry
IKKβ	Inhibitor of nuclear factor kappa B kinase subunit beta
IL	Interleukin
INDEL	Insertion/Deletion
JAK	Janus kinase
KRAS	Kirsten rat sarcoma virus
LCC	Large-cell carcinoma
LPS	Lipopolysaccharide
LRP1B	LDL receptor related protein 1B
LUSC	Lung squamous-cell carcinoma
MAPK	Mitogen-activated protein kinase
MHC	Major histocompatibility complex
MDSC	Myeloid-derived suppressor cells
MEK	Mitogen-activated protein kinase
mTOR	Mechanistic target of rapamycin
MTT	3-[4,5-dimethylthiazol-2-yl]-2,5 diphenyl tetrazolium bromide
NEMO	NF-κB essential modulator

NF-κB	Nuclear factor kappa B
NK	Natural killer cells
NKX2-1	NK2 homeobox 1
NSCLC	Non-small cell lung cancer
NSG	NOD scid gamma
OTU	Ovarian tumor
OVA	Ovalbumin
PCR	Polymerase Chain Reaction
PD-1	Programmed cell death protein 1
PD-L1	Programmed cell death-ligand 1
PDK1	Pyruvate dehydrogenase kinase 1
Pi3K	Phosphatidylinositol-3-kinase
PROTAC	Proteolysis-targeting chimera
PRR	Pattern recognition receptors
RAF	Rapidly accelerated fibrosarcoma kinase
RAS	Rat sarcoma virus
RB	Retinoblastoma protein
RGS	Regulator of G-protein signaling
RIP1	Receptor interacting protein 1
RNA	Ribonucleic acid
RNS	Reactive nitrogen species
ROS	Reactive oxygen species
RT-qPCR	Real-time quantitative PCR
RTK	Receptor tyrosine kinase
SCLC	Small cell lung cancer
SDS-PAGE	Sodium dodecyl sulfate-polyacrylamide gel electrophoresis
SHS	Second-hand smoke
siRNA	Small interfering RNA

SMAD	Homologs of drosophila mothers against decapentaplegic (Mad) and Caenorhabditis elegans Sma
SNP	Single nucleotide polymorphisms
SOS	Son of sevenless
STAT	Signal transducers and activators of transcription
TAK1	Transforming growth factor-β-activated kinase 1
TAM	Tumor associated macrophage
TAP	Transporter associated with antigen processing 1
TBK1	TANK-binding kinase 1
TetO	Tet operator sequences
TGF	Transforming growth factor-alpha
TIDE	Tracking of indels by decomposition
TKI	Tyrosine kinase inhibitor
TMB	Tumor mutational burden
TME	Tumor microenvironment
TNF-α	Tumor necrosis factor alpha
TNFAIP3	TNF alpha induced protein 3
TNFR	Tumor necrosis factor receptor
Tregs	Regulatory T cells
tTA	Tetracycline-controlled transactivator
TP53	Tumor protein p53
VEGF	Vascular endothelial growth factors
VST	Variance-stabilizing transformation
ZnF	Zinc-finger

Introduction

Cancer: a global health challenge

Cancer is the second leading cause of death worldwide. In 2022, the World Health Organization reported an estimated 20 million new cancer cases and 9.7 million cancer-related deaths.[1] Approximately one in five people develop cancer throughout their lifetime and despite major advancements in treatment, roughly one in eleven patients die from the disease.[2] A recent study projects a major rise in global cancer burden with 35.3 million cancer cases worldwide, an increase of 76.6% by 2050.[3] This sharp rise is linked to a growing world population and a shift in demographics towards aging populations in high-income countries, as 60% of cancers occur in people aged 65 years or older.[4,5] Environmental risks, such as exposure to air pollution and carcinogens as well as lifestyle factors like smoking, alcohol consumption, diet, physical activity, and obesity greatly contribute to global cancer incidence.[6,7] With the growing prevalence of cancer in the future there is an urgent need for a better understanding of cancer biology and the development of new cancer therapies.

Lung Cancer Epidemiology

In 2022, lung cancer was the most frequently diagnosed type of cancer, accounting for 2.5 million new cases (12.4% of all cancers) globally. With 1.8 million deaths, lung cancer contributed to 18.7% of all cancer-related deaths in the same year, making it the main contributor to cancer fatalities worldwide.[1] Tobacco use is responsible for approximately 85% of all lung cancer cases and is considered the most preventable cause of cancer.[8] While most cases of lung cancer can be linked to tobacco consumption, exposure to environmental factors, genetic factors, such as chromosomal abnormalities, mutation of oncogenes or tumor-suppressors, or dysregulation in microRNAs all contribute to lung cancer risk.[9] In addition, heritable factors can further increase lung cancer risk. Familial cancers may occur more frequently in some families due to inheritance of potentially carcinogenic mutations.[10]

Etiology

Tobacco consumption

Worldwide, around 1.3 billion people smoke tobacco regularly, despite the well-known connection between smoking and lung cancer. Nonetheless, this awareness contributed to positive trends towards cancer prevention by a steady decline in the proportion of the global smoking population since the 1980s.[11,12] Even though addiction to nicotine is the main reason for people to smoke tobacco products it is not considered a carcinogen. Tobacco smoke consists of more that 5000 compounds, 73 of which show evidence of carcinogenic potential. Smoking induces pulmonary inflammation, which can play a key role in carcinogenesis.[13] Carcinogenic components of tobacco smoke can interact with DNA, either directly or after metabolic modification, to form covalently bound DNA adducts. The consequence of smoke-induced DNA adducts is the induction of DNA mutations. Indeed, studies have revealed that lung cancers show a particularly high number of somatic mutations.[14] The high mutation rate increases the likelihood of induction of mutations in critical tumor suppressor genes and oncogenes, such as tumor protein p53 (*TP53*), Kirsten rat sarcoma virus (*KRAS*) and epidermal growth factor receptor (*EGFR*), among others.[15]

Air pollution and occupational hazards

Although tobacco smoke is the most common reason for lung cancer, it is not the only significant one. While smoking-related lung cancer cases have decreased in many countries, the incidence in non-smokers has risen, due to environmental and occupational exposure to carcinogenic substances.[16] Air pollution is a general global health problem, including but not limited to lung cancer. More people than ever are exposed to air pollution due to economic development and an increase in urbanization.[17] Outdoor air pollution includes particulate matter from vehicular and industrial exhausts, toxic metals, asbestos, or microorganisms. Indoor air pollution includes cooking fumes, second-hand smoke (SHS), and carcinogens in home decorating materials such as formaldehyde, ammonia, and radon.[18] SHS increases the risk of developing lung cancer by 20–24% and contributes to 16–24% of lung cancer cases in non-smokers.[19]

Genetic predispositions

Less than 20% of smokers develop lung cancer during their lifetime. Combined with the increased lung cancer risk in non-smokers with a family history of cancer, this highlights the importance of genetic factors in tumorigenesis. Certain genetic variants pose a significantly higher lung cancer risk. Fine mapping studies have revealed a significant susceptibility to lung cancer at locus 6q23–25 and identified regulator of G-protein signaling 17 (*RGS17*) which encodes a member of the regulator of G-protein signaling (RGS) family as a likely candidate gene.[20,21] Furthermore, 21 additional genes have been linked to lung cancer predisposition, DNA-(apurinic or apyrimidinic site) lyase (*APEX1*), ATM serine/threonine kinase (*ATM*), and C-X-C motif chemokine receptor 2 (*CXCR2*) being among the most significant ones.[20] Genetic variants associated with lung cancer risk include single nucleotide polymorphisms (SNPs), insertions/deletions (INDELs), copy number variations, epigenetic alterations, chromatin structure variations, and microsatellite instability.[22–24]

Pathogenesis and Progression

As in other types of cancer, lung cancer cells exhibit defects in homeostasis and uncontrolled proliferation. The transformation from a healthy cell to a malignant lung cell occurs in a multi-step fashion by acquiring several genetic and/or epigenetic lesions, such as mutations activating proto-oncogenes as well as mutations deactivating tumor suppressor genes. The most common mutations in lung cancer occur in the oncogenes *KRAS*, *EGFR*, anaplastic lymphoma kinase (*ALK*), *Myc* (c-Myc, N-Myc, L-Myc) or the tumor suppressor gene *TP53.* By the time lung cancer becomes detectable as many as 10-20 mutations may have already occurred.[25] Accumulation of mutations leads to dysregulation of proliferation and clonal expansion of malignant cells, leading to the formation of a primary tumor in the lung tissue. For the tumor to metastasize, cells must acquire the ability to invade the stroma and enter the bloodstream or lymphatic vessels. This includes epithelial-mesenchymal transition (EMT), a process in which cells convert from epithelial cells to mesenchymal cells, typically seen in embryonic development. The most frequent metastatic sites for lung cancer are the nervous system, bones and liver. In later stages, tumor growth may lead to organ failure, ultimately contributing to the patient's death.[26,27]

Classification of Lung cancer

Lung cancer can be divided into two main categories, small-cell lung cancer (SCLC), which accounts for roughly 15% of all lung cancer cases, and non-small cell lung cancer (NSCLC), which accounts for approximately 85% of all lung cancer cases. SCLC tumors arise from malignant neuroendocrine cells upon loss of the tumor suppressors retinoblastoma protein (*RB*) or *TP53*. NSCLC on the other hand emerges after distinct genetic events in lung epithelial cells. NSCLC is further divided into three sub-types, based primarily on tumor cell morphology: lung adenocarcinoma (LUAD), lung squamous-cell carcinoma (LUSC) and large-cell carcinoma (LCC).[28,29] Alongside cell morphology, the origin of the tumor cells contributes to this classification. It is widely recognized that LUAD derives from alveolar type II epithelial cells or cells located in bronchioalveolar duct junctions.[30] LUSC develops from basal epithelial cells in the airways and LCC derives from various types of lung epithelial cells.[29] LUAD is the most common subtype, accounting for 40% of all lung cancer cases, followed by LUSC with 25% and LCC with 10% of all lung cancers.[31] However, this has not always been the case. Since the late 1990s the proportion of LUAD in lung cancer cases has been rising steadily, while the proportion of LUSC has declined. This shift has been associated with several different factors, such as the introduction of filtered cigarettes which allow deeper smoke inhalation and peripheral distribution of smoke, increased air pollution and people quitting smoking at a younger age.[32] Lung cancer types like SCLC or LUSC are typically more closely linked to smoking whereas LUAD is the most common subtype among non-smokers with other environmental and genetic factors playing a major role in its development.[33]

Molecular Drivers of Lung adenocarcinoma

LUAD is driven by a range of different genetic alterations. Copy number analysis of LUAD tumors revealed large-scale copy number gains and losses which contribute to the disease's progression. The most frequent event, a recurrent amplification of chromosome region 14q13.3 was found in 12% of the analyzed samples. Within this region lies NK2 homeobox 1 (*NKX2-1*), a transcription factor critical for lung development.[34] Several epigenetic alterations have also been shown to affect LUAD tumorigenesis, such as hypermethylation of the cyclin-dependent kinase inhibitor 2A

(*CDKN2A*) promoter or lower global levels of histone acetylation.[35] The mutation profile of LUAD significantly differs from other subtypes of NSCLC. The most frequently mutated genes in LUAD include the tumor suppressor genes *TP53* (51.3%), LDL receptor related protein 1B (*LRP1B*) (30.3%) and the oncogenes *KRAS* (29.1%), *EGFR* (14.2%) and *BRAF* (7.2%).[36,37] These mutations are differentially distributed in tumors based on sex and smoking status of the patient. For instance, mutations in *KRAS* are more commonly found in patients with a history of heavy smoking than *EGFR* mutations. On the other hand, LUAD with mutations in *EGFR* are more common in women than men.[38,39]

Oncogenic Mutations in EGFR and KRAS in NSCLC

EGFR is a transmembrane receptor, belonging to HER/erbB family of receptor tyrosine kinases (RTKs), which includes HER1, HER2, HER3 and HER4. It plays a prominent role in regulating fundamental processes in mammalian cells, such as growth, proliferation, survival and differentiation. EGFR consists of several functional domains: an extracellular ligand binding domain, a transmembrane helix and an intracellular domain with tyrosine kinase activity. EGFR has seven known ligands, which include the high-affinity ligands epidermal growth factor (EGF), heparin-binding EGF-like growth factor (HBEGF), transforming growth factor-alpha (TGF-α), and betacellulin (BTC).[40] Ligand binding induces conformational changes in the receptor, resulting in dimerization and further downstream signaling (Fig. 1).[41,42] EGFR signaling includes activation of the Pi3K-PDK1-AKT-mTOR and the Janus kinase (JAK) – signal transducers and activators of transcription (STAT) pathway. Additionally, EGFR is an upstream activator of the RAF-MEK-ERK pathway via KRAS. Target genes of EGFR signaling are involved in proliferation, cell cycle progression and cell growth.

KRAS is part of the *RAS* gene family, encoding for small GTPases that serve as molecular switches in pathways, downstream of EGFR signaling. They are essential for control of cell proliferation and survival. RAS proteins can exist in an active GTP-bound, and an inactive, GDP-bound state, transitioning between these two forms. Their activation and deactivation are regulated by ras guanine nucleotide exchange factors (GEFs) and ras GTPase-activating proteins (GAPs) respectively. GEFs trigger activation by promoting the exchange of GDP for GTP, while GAPs enhance the RAS-

intrinsic GTPase ability, causing conversion of GTP to GDP, thereby inactivating RAS.[43,44] Activation of KRAS is triggered by extracellular stimuli like growth factor binding to RTKs. Growth factor binding and the subsequent dimerization of two receptors, results in activation of the kinase activity in the intracellular domain. The kinase activity catalyzes autophosphorylation of tyrosine residues, providing binding sites for adaptor proteins such as growth factor receptor-bound protein 2 (GRB2). GRB2 recruits Son of sevenless (SOS), a part of the GEF family, which promotes exchange of GDP to GTP on KRAS proteins, thereby activating it.[45] Activation of KRAS can lead to initiation of several different downstream signaling cascades.

Mutations in EGFR are the second most common oncogenic drivers in NSCLC. Approximately 85–90% of EGFR mutations are activating mutations, such as the exon 19 deletion or point mutations like L858R, G719S, L861Q in exons 19 or 21. Less frequent mutations include point mutations, insertions, and deletions in exons 18–25 of *EGFR.*[41,46] EGFR mutations can occur in the extracellular region, the juxtamembrane region or in the kinase domain, all of which lead to a constitutively activated receptor, constantly driving downstream signaling.[47]

On the other hand, mutations in KRAS are the most common oncogenic driver in LUAD. Most mutations occur in codon 12, with G12C (40%) and G12D (22%) being the most common amino acid substitutions. Less common are mutations in codon 13 and rarely in codon 61. Nucleotide transversions like the ones in $KRAS^{G12C}$ and $KRAS^{G12D}$ are associated with exposure to tobacco smoke and are more common in smokers than non-smokers.[48] Oncogenic mutations in KRAS lead to a gain-of-function, constitutively activating the protein, which results in activation of its downstream pathways in a ligand-independent manner.[49] KRAS mutations influence the binding affinity to different downstream signaling molecules, determining the primary pathway involved in tumorigenesis. $KRAS^{G12D}$ and $KRAS^{G12C}$ reportedly bind to both phosphatidylinositol 3-kinase (Pi3K) and rapidly accelerated fibrosarcoma kinase (RAF), in contrast to $KRAS^{G12R}$, which binds to RAF but has impaired affinity to Pi3K.[50,51]

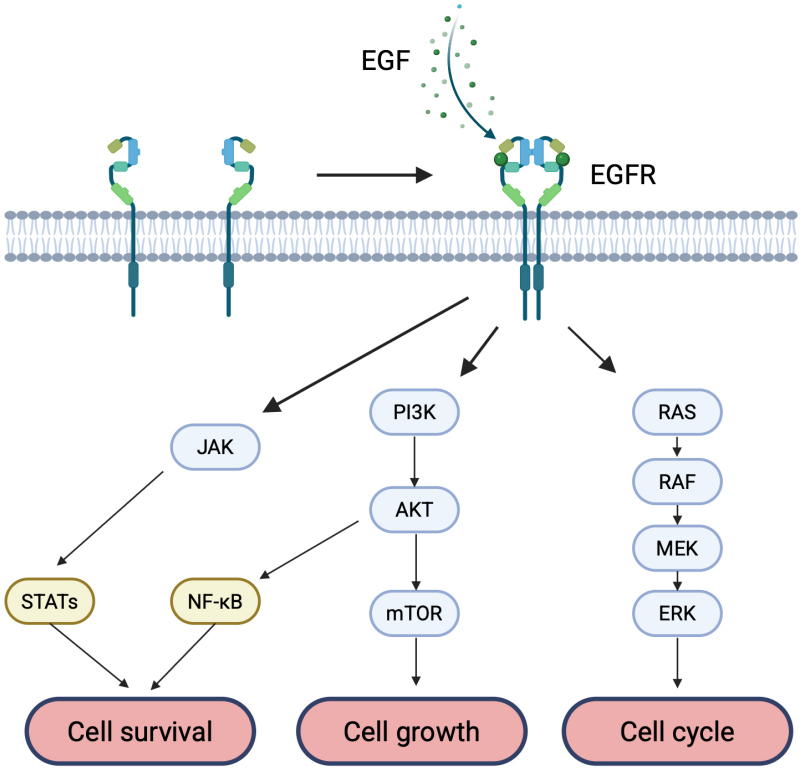

Figure 1: EGFR signaling pathway: Upon receptor binding of EGF to EGFR, EGFR monomers dimerize and initiate downstream signaling pathways via RAS, Pi3K and JAK-STAT signaling. EGFR signaling induces target gene expression of genes involved in cell survival, cell growth and cell cycle regulation. Adapted from *Sung et al.*[52] Created with BioRender.com

Targeted Therapy in EGFR- and KRAS-Driven LUAD

The identification of EGFR and KRAS as major players in lung tumorigenesis has fueled the development of targeted therapeutic approaches. Chemotherapy remains a first-line treatment for patients with EGFR-mutant LUAD, but combination with targeted therapy is supported for patients with stage IV LUAD. Tyrosine kinase inhibitors (TKIs) specifically target EGFR with activating mutations and are divided into four generations.[53] Erlotinib and gefitinib belong to the first generation of TKIs. These compounds reversibly bind to EGFR and inhibit adenosine triphosphate (ATP) binding to the tyrosine kinase domain. 50–60% of tumors treated with first generation TKIs, however, develop resistance within 9–12 months, primarily via the T790M mutation.[54] Second generation TKIs, like afatinib irreversibly bind to EGFR and are more potent than first generation TKIs but tend to have more severe side effects and remain ineffective against the T790M resistance mutation. Due to the limitations of first- and

second-generation TKIs in circumventing T790M resistance, third-generation TKIs have been developed. Third-generation TKIs have significantly higher activity in EGFR-mutant cells, making them specific to tumor cells. The first U.S. Food and Drug Administration (FDA)-approved third generation TKI, osimertinib, irreversibly targets the L858R and the most common evasion mutation T790M, while not inhibiting wild-type (WT) EGFR.[55] Osimertinib is used as first-line treatment for patients with sensitizing EGFR mutations and as second line treatment for patients with the T790M resistance mutation. Despite encouraging initial responses in patients, resistance to osimertinib inevitably develops either through on-target resistance mechanisms, such as other acquired mutations in EGFR (e.g. C797S) or through off-target mechanisms, involving downstream EGFR signaling components.[56,57] Since 2019 osimertinib is included as a first-line treatment option for EGFR-positive patients by the USA National Comprehensive Cancer Network guidelines.[58] The use of first- and second generation TKIs has since declined, because the indication for osimertinib as a second-line treatment is limited for patients with metastatic NSCLC with $EGFR^{T790M}$ mutation after their disease progressed following an earlier TKI treatment.[59] For on-target resistance, a fourth-generation of TKIs, targeting mutations like C797S is emerging as a therapeutic option, however no fourth-generation TKI has been clinically approved so far.[60]

In contrast, targeting KRAS has historically been a greater challenge. First-line treatment commonly consists of chemotherapy and immune checkpoint blockade (ICB) therapy. Immune checkpoints are molecules that either promote or inhibit T cell activation. ICB therapy targets these molecules to promote T cell priming or to inhibit negative signals. Blocking negative signals, like cytotoxic T-lymphocyte–associated antigen 4 (CTLA-4), or programmed cell death protein 1 (PD-1) delays or even prevents T cell silencing and have shown to improve the survival of patients with solid cancers.[61] While the use of immune checkpoint inhibitors (ICIs) has shown clinical benefits in some patients, the response in some patients with KRAS-mutant NSCLC is still poor.[62] RAS proteins were previously believed to be “undruggable”, due to their structural and biochemical properties. KRAS binds GTP with a high affinity, in the picomolar range, requiring more potent inhibition than traditional blockers provide. Secondly, KRAS does not exhibit clear pockets that could serve as binding sites for small inhibitor molecules.[63] Therefore, other molecular pathways were identified and

targeted. Farnesyltransferase inhibitors, which block farnesylation of RAS (critical for activating Ras) were developed, but tumor cells developed resistance by signaling through other pathways. Furthermore, upstream and downstream targets of RAS were targeted, such as EGFR by Tyrosine Kinase Inhibitors (TKIs) or mitogen-activated protein kinase (MEK) with MEK inhibitors. These efforts however showed rather disappointing results.[64] In 2013 *Ostrem et al.* reported on a pocket, not apparent in previous structural studies of $KRAS^{G12C}$, and demonstrated that binding of this pocket disrupts binding to RAF.[65] This finding marked a breakthrough, as only eight years later the FDA approved the first KRAS inhibitor sotorasib. Combination of targeted therapy with ICB has shown promising results, however, toxicity and acquired resistance remain major challenges.[64]

Chronic Inflammation and Tumor infiltrating immune cells in Lung Cancer

About 25% of human cancers are related to inflammation or microbial infections. The lung is exposed to environmental stressors such as tobacco smoke and air pollution and is sensitive to injury and inflammation. As a response to irritants in smoke or polluted air immune cells, including macrophages, neutrophil granulocytes, and T lymphocytes are activated and release a variety of pro-inflammatory cytokines (e.g. tumor necrosis factor alpha (TNF-α) and interleukins IL-1, IL-6, IL-8).[66] Chronic activation of these immune cells can lead to an accumulation of reactive oxygen/nitrogen species (ROS/RNS), which can induce DNA damage, inhibit apoptosis and activate proto-oncogenes by initiating signal transduction pathways.[67] The release of cytokines and chemokines not only plays a role in the inflammatory response but also promotes tumor progression. IL-6 for example, produced by tumor cells, stromal cells or immune cells, can inhibit apoptosis, increase ROS, or activate pathways involved in proliferation, cell migration and angiogenesis.[68] Pro-inflammatory stimuli such as TNF, IL-1 or lipopolysaccharide (LPS) activate inflammatory pathways such as the NF-κB pathway. Through persistent cytokine signaling and oxidative stress chronic inflammation also promotes infiltration of immune cells into the tumor microenvironment (TME). During cancer development the inflammatory cell population continuously changes. Tumor infiltrating immune cells can significantly alter tumor progression due to their pro- or anti-inflammatory

properties. Tumor-associated macrophages (TAMs) can adopt different polarization states: M1-like macrophages exhibit a pro-inflammatory phenotype by secreting ROS and cytokines like IL-6, IL-12, IL-23, and TNF-α. They exhibit high antigen presenting capacities and are generally regarded as anti-tumorigenic. M2-like TAMs on the other hand are usually associated with tissue repair. In a cancer context however they are generally considered to be pro-tumorigenic due to their support in angiogenesis by secreting adrenomedullin and vascular endothelial growth factor (VEGF) and the expression of immunosuppressive molecules, like PD-L1 and TGFβ, promoting tumor progression and immune evasion. Macrophage polarity, however, is widely considered to be a spectrum, rather than a strict binary and therefore cannot be fully explained by the simplistic M1-M2 dichotomy.[69] Tumor infiltrating T lymphocytes, most notably $CD4^+$ T cells and $CD8^+$ T cells, execute important cytotoxic functions in the TME. $CD4^+$ T cells have different effects in cancer progression depending on the subtype. $CD4^+$ T helper 1 (Th1) cells activate $CD8^+$ T cells by secreting Interferon gamma (IFN-γ), thereby contributing to anti-tumor immunity. $CD4^+$ regulatory T cells (Tregs) on the other hand, suppress immune responses and are therefore associated with tumor immune evasion.[70,71] $CD8^+$ cytotoxic T cells target tumor cells for destruction by secreting perforin and granzyme B.[72]

A20 as a negative feedback regulator of NF-κB signaling

A20, also known as tumor necrosis factor alpha-induced protein 3 (TNFAIP3), was first identified as a TNF-inducible response gene in endothelial cells. A20 was originally thought to be an inhibitor of TNF-induced apoptosis. Follow-up studies, however, revealed A20s role as an inhibitor of the NF-κB pathway activation through TNF, IL-1, IL-17, CD40, pattern recognition receptors (PRRs) and T and B cell receptor activation.[73] Upon initiation of the canonical NF-κB pathway, binding of pro-inflammatory cytokines such as TNF-α or IL-1β to their respective receptors triggers nuclear translocation of NF-κB subunits and initiate gene expression of target genes, including *TNFAIP3*, which encodes for A20.[74] A20 is an enzyme that possesses both E3 ubiquitin ligase and deubiquitinating activity. It consists of a highly conserved sequence of 790 amino acids comprising an amino-terminal ovarian tumor (OTU) domain and seven carboxy-terminal zinc-finger (ZnF) domains. The OTU domain

exhibits deubiquitinating activity, while the ZnF domains support E3 ubiquitin ligase and ubiquitin-binding activities.[75] A20 is a negative feedback regulator in the TNF-induced NF-κB pathway and inhibits signaling by multiple mechanisms. Upon A20 expression, the enzyme removes K63-linked polyubiquitin chains from Receptor Interacting Protein 1 (RIP1), preventing its interaction with NF-κB essential modulator (NEMO). In a second step A20 adds K48-linked polyubiquitin chains to RIP1, targeting it for proteasomal degradation.[76] This prevents the phosphorylation of inhibitor of NF-κB kinase subunit β (IKKβ), thereby hampering canonical NF-κB signaling (Fig. 2).[77] Additionally, A20 regulates IFN signaling,[78] transforming growth factor β (TGFβ) mediated SMAD (homologs of Drosophila mothers against decapentaplegic (Mad) and *Caenorhabditis elegans* Sma) activation,[79] and inhibits apoptosis and autophagy in certain cell types.[80]

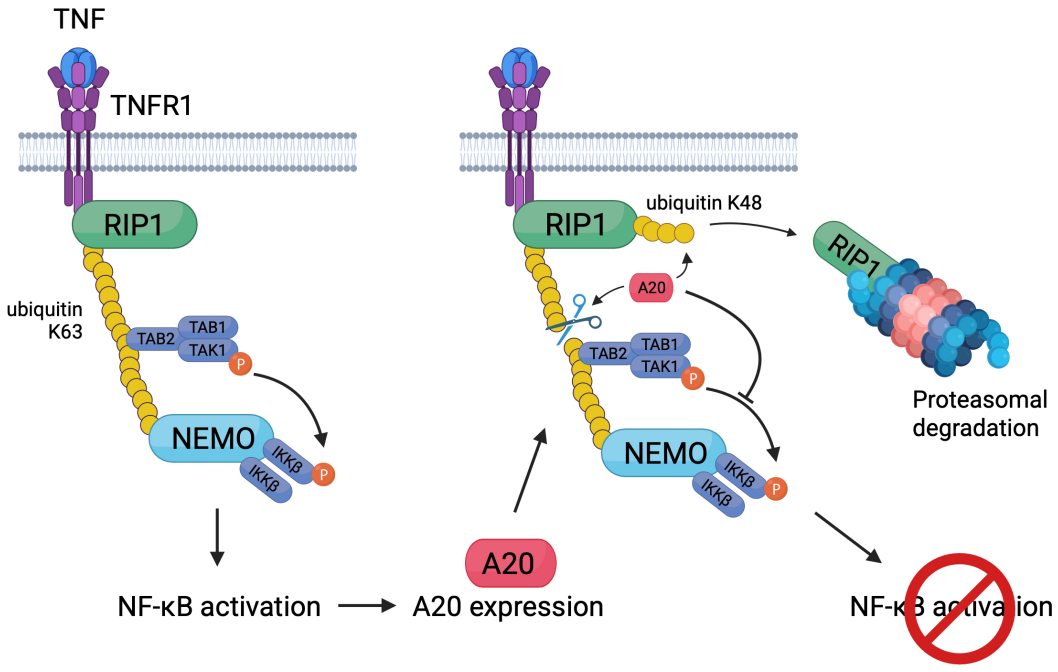

Figure 2: Schematic mechanism of A20-mediated NF-κB inhibition. TNF binding to TNF-receptor 1 (TNFR) RIP1 is poly-ubiquitinated on K63. The ubiquitin chain serves as a scaffold for the recruitment of the Transforming growth factor-β-activated kinase 1 (TAK1) complex and the IκB kinase (IKK)-NEMO complex. TAK1 phosphorylates IKKβ leading to downstream NF-κB activation and expression of NF-κB target genes, including A20. A20 subsequently cleaves K63-linked polyubiquitin chains on RIP1 and tags it with K48-linked polyubiquitin chains for proteasomal degradation. Additionally, A20 destabilizes the IKK-NEMO complex by binding to NEMO and blocking the phosphorylation of IKKβ. Adapted from *Catrysse et al.* [73] Created with BioRender.com

The dual role of A20 in cancer

Human genetic studies have linked germline SNPs in *TNFAIP3* to susceptibility to a variety of diseases including rheumatoid arthritis, systemic lupus erythematosus, type 1 diabetes, coeliac disease, Crohn's disease and more.[81] Apart from inflammation-related diseases, aberrant A20 can also lead to malignancies. Initially, biallelic somatic mutations in A20 were found in about 30% of human B cell lymphomas.[82] Furthermore, A20's role in different human cancers such as pancreatic cancer, T cell lymphoma, leukemia, and lung cancer was investigated. While in some cancers (B cell lymphomas, colorectal carcinomas, and hepatocellular carcinomas) A20 displays tumor suppressive properties, in other cancers (breast cancer, gastric cancer, and melanoma), A20 has an oncogenic role in tumorigenesis and tumor progression.[83] Regarding lung cancer, *in vitro* experiments showed that the microRNA-605-5p downregulated the expression of A20, which led to increased invasion and proliferation of NSCLC cells.[84] In addition, A20 suppressed NF-κB activity and reduced resistance to apoptosis induced by KRAS mutations in NSCLC.[85] These studies hinted towards a tumor suppressive role of A20 in NSCLC. Indeed, a study conducted by our laboratory found that the loss of A20 activated the TANK-binding kinase 1 (TBK1)-STAT1-PD-L1 axis, facilitating tumor evasion from $CD8^+$ T cell-mediated immune surveillance, thereby validating A20 as a potent tumor suppressor in KRAS-driven LUAD.[86]

A20 in KRAS-driven lung adenocarcinoma

In the study conducted by our lab we found shallow deletions of *TNFAIP3* in 55.4% of patients harboring KRAS-driven LUAD while deep deletions were identified in 1.3% of patients' tumors.[86] These genetic alterations resulted in reduced A20 mRNA expression in KRAS-mutant LUAD tumors compared to healthy lung parenchyma. The same reduction in A20 mRNA expression was observed in EGFR-mutant tumors, suggesting that tumors commonly downregulate A20 expression to enhance NF-κB signaling, thereby sustaining a pro-tumorigenic inflammatory response. Additionally, we associated a low tumor-intrinsic A20 expression with worse prognosis in patients. With *in vivo* experiments the study showed that mice harboring A20-deficient $KRAS^{G12D}$ tumors, as well as A20 heterozygous $KRAS^{G12D}$ tumors, exhibited

decreased survival compared to mice with A20-expressing $KRAS^{G12D}$ tumors. It was concluded that tumor-intrinsic loss of A20 creates a pro-tumorigenic TME, as a reduced $CD8^+$ T cell infiltration and M1-polarized macrophages, but increased abundance of M2-polarized macrophages and Tregs was observed. Loss of A20 was correlated with an increased TBK1 phosphorylation, resulting in autocrine IFN signaling and enhanced STAT1 activation, which leads to an upregulation of PD-L1 expression in tumor cells, contributing to enhanced immune evasion. Increased IFN signaling had previously been associated with a better response of patients to anti-PD-/PD-L1 ICB,[87] and indeed, *in vivo* experiments revealed that mice harboring A20-deficient tumors responded better to α-PD-L1 ICB therapy by restoring T cell infiltration in the TME resulting in improved survival and a lower tumor burden. These findings demonstrate A20's important role as a tumor suppressor in KRAS-driven LUAD, that may be used as a predictive biomarker to improve the efficacy of ICB therapy in patients, as lower A20 expression leads to an increased PD-L1 expression in tumor cells, making them more susceptible to α-PD-L1 therapy.[86]

A20 in EGFR-driven lung adenocarcinoma

EGFR tumors typically exhibit an immune-cold phenotype compared to KRAS tumors, characterized by poor infiltration of immune cells, including $PD\text{-}L1^+/CD8^+$ tumor-infiltrating T cells.[88] This creates an immunosuppressive TME with low tumor immunogenicity and higher proportions of suppressive TAMs, Tregs and myeloid-derived suppressor cells (MDSCs).[89–91] Clinical trials suggest that the "cold" phenotype of EGFR tumors likely contributes to a poor response to ICB treatment with PD-1/PD-L1 inhibitors.[92] However, new evidence suggests that a subset of patients may still benefit from ICB therapy, depending on specific biomarkers reflecting the TME. For example, a study examining the ICB therapy response of NSCLC patients found that those with a high tumor mutational burden (TMB) yielded significantly improved, durable treatment results compared to patients with low TMB tumors.[93] Studies like this underscore the significance of testing specific biomarkers in molecular diagnosis to determine an appropriate therapeutic strategy for individual patients with EGFR-mutant LUAD. One such biomarker may be A20, as it is a key regulator of inflammation, which substantially contributes to shaping the TME. Since the

composition of the TME plays a pivotal role in the efficacy of immunotherapy,[94] a better understanding of molecular inflammation regulators may reveal new therapeutic opportunities. As previously described, loss of A20 was already shown to render KRAS-mutant tumors more susceptible to ICB *in vivo*.[86] Further examination of the role of A20 in EGFR-mutant LUAD may aid in the development of novel therapeutic options targeting this type of cancer.

In our previous study we showed that downregulation of A20 expression occurs in both KRAS- and EGFR-mutant LUAD, compared to healthy tissue (Fig. 3A), suggesting that A20 may also act as a tumor suppressor in EGFR-driven LUAD.[86] Kaplan-Meier survival analysis using an autochthonous mouse model of $EGFR^{L858R}$:Δp53 (EP) tumors showed an increased survival to $EGFR^{L858R}$:Δp53:ΔA20 (EPA) tumors (Fig. 3B). In these mouse models, the TMB is typically lower than in their human counterparts by an order of magnitude, as lung cancers are characterized by a high TMB.[95] The result of a low TMB is a limited neoantigen presentation by tumor cells, leading to a lack of immune cell infiltration in the TME. To better model human-like TME conditions, chicken ovalbumin (OVA) was introduced as a neoantigen in the autochthonous model, to ensure immune recognition of tumor cells. Interestingly mice with $EGFR^{L858R}$:Δp53:ΔA20:OVA (EPOA) tumors exhibited improved survival compared to $EGFR^{L858R}$:Δp53:OVA (EPO) (Fig. 3D). This finding suggests that the loss of A20 leads to a shift from a tumor suppressor to an oncogene in immunogenic EGFR-tumors, in contrast to OVA-expressing KRAS-driven tumors, where loss of A20 did not change the survival outcomes (Fig. 3C). Furthermore, mice with EPOA tumors have a significantly reduced tumor burden compared to A20 proficient EPO and OVA-deficient EP and EPA tumors (Fig. 3E, 3F). These findings hint towards a pivotal role of A20 in the modulation of tumor immunogenicity and could provide new possibilities to treat EGFR-mutant LUAD. Based on the previous findings, we hypothesized a potential oncogenic role of A20 in EGFR-driven LUAD. Since A20 was previously shown to be an important modulator of TME remodeling and T cell infiltration in KRAS-driven LUAD, we speculated that it might play an opposite role in the instance of immunogenic EGFR-driven LUAD. This hypothesis was supported by the observation that loss of A20 correlated with increased survival and reduced tumor burden in mice bearing immunogenic EGFR-driven tumors. These findings suggest a strong link between A20 activity and the TME.

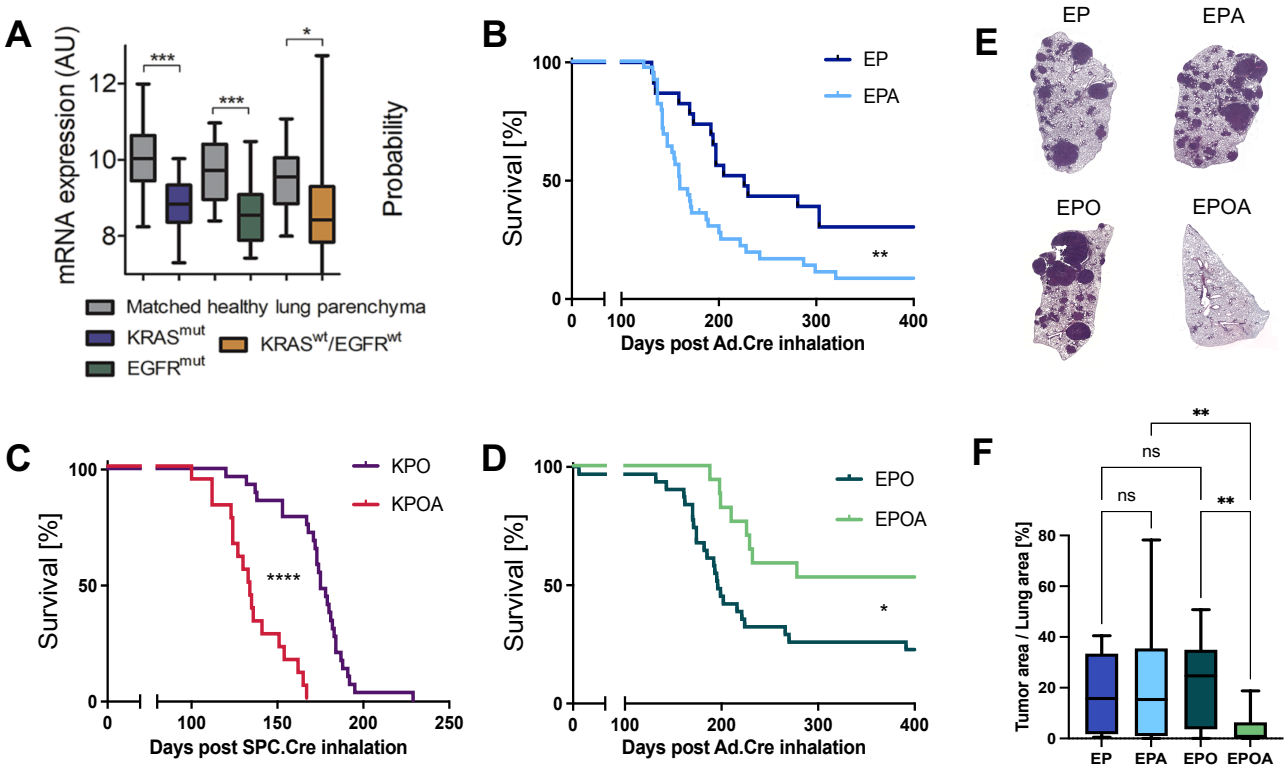

Figure 3: (A) A20 mRNA expression KRAS mutant, EGFR mutant and KRAS wild-type/EGFR wild-type LUAD biopsies compared to adjacent healthy lung tissue (from *Breitenecker et al.*).[86] Survival analysis of **(B)** $EGFR^{L858R}$:Δp53 (EP) versus $EGFR^{L858R}$:Δp53:ΔA20 (EPA); **(C)** $KRAS^{G12D}$:Δp53:OVA (KPO) versus $KRAS^{G12D}$:Δp53:ΔA20:OVA (KPOA); **(D)** $EGFR^{L858R}$:Δp53:OVA (EPO) versus $EGFR^{L858R}$:Δp53:ΔA20:OVA (EPOA) post intranasal inhalation of Ad.Cre. **(E)** Images of representative H&E stained sections of mouse lungs with EP, EPA, EPO and EPOA tumors. **(F)** Tumor area to lung area ratio of mouse lungs with EP, EPOA, EPO and EPOA tumors. *P < 0.05, **P < 0.01, ***P < 0.001, ****P < 0.0001.

Aim of the Thesis

The aim of this thesis is to investigate the role of A20 in EGFR-mutant tumors. Since A20 is an important player in shaping the TME, a key objective is the characterization of the TME to understand A20's impact on immune cell infiltration into tumors and tumor progression. Additionally, A20-deficient human EGFR-mutated LUAD cells will be characterized *in vitro* to investigate their growth, expressed signaling pathways and sensitivity to TKIs. This project aims to provide insights into EGFR-LUAD dynamics, that could contribute to the design of new therapeutic approaches for patients.

Materials and Methods

Material List

Materials	Company	Catalogue No.
Acetic acid	Merck	71183
Acrylamide/Bis-acrylamide (30%)	Carl Roth	A124.1
Agarose	Sigma-Aldrich	A9539
Ammonium–chloride–Potassium (ACK) buffer	Lonza	BP10-548E
Ampicillin	Sigma-Aldrich	A9518-5G
Anti-mouse CD16/32 (Fc-block)	BD Biosciences	553142
Anti-polyvalent biotinylated antibody	ScyTek Labs	ABN005
APS	Thermo-Scientific	A3678
Aquatex	Merck	108562
Avidin blocking solution	ScyTek Labs	BBK030
BCA protein assay kit	MyBioSouce	MBS841734
Biotin blocking solution	ScyTek Labs	BBK030
Biotin Chromogen	ID labs	BP1108
BSA standard solution	Thermo-Scientific	23209
Cell strainer 70 µm	Corning	352350
Citrate buffer pH6	Agilent DAKO	S2369
Citrate buffer pH9	Agilent DAKO	S2367
DNase I	Thermo-Scientific	EN0521
Doxycycline	Sigma-Aldrich	D5207
E.Z.N.A.® Total RNA Kit I	OMEGA Bio-tek	M6399-01
EDTA	Chem-Lab NV	CL00.0554.0500
EGTA	ITW Reagents	A0878,0025
Ethanol ≥99,5%	Carl Roth	5054.1
FastDigest BpII	Thermo-Scientific	FD1014
FavorPrep™ PCR Clean Up Kit	Favorgen	FAPCK 001-2
FBS	Capricorn Scientific	FBS-12A
Gene Ruler 1 kb	Thermo-Scientific	SM0312

Glycerol-2-phosphate	Sigma-Aldrich	G9422
Glycine	Carl Roth	3187.3
GoTaq® G2 DNA Polymerase kit	Promega	M7841
GoTaq® qPCR Kit	Promega	A6010
H_2O_2 solution (30%)	ITW Reagents	121076.1211
Hard-Shell® 96-Well PCR Plates	BioRad	HSP9601
Hematoxylin	Sigma-Aldrich	1.09249.1000
High Pure Plasmid Isolation Kit	Roche	11754785001
Histofix	Carl Roth	P087.1
IFN-γ	ImmunoTools	12343534
Il-6	ImmunoTools	12340062
iScript™ cDNA synthesis kit	BioRad	1708890
Isopropanol	Carl Roth	6752.3
jetOPTIMUS® transfection kit	Polyplus	101000051
Ketamine (Ketamidor)	VetViva	57446/5005
LPS	Thermo-Scientific	00-4976-93
M.O.M.® (Mouse on mouse blocking reagent	Vector Labs	BMK-2202
MTT-Assay Kit	R&D Systems	4890-025-K
Na_3VO_4	Sigma-Aldrich	567540
NaCl	Sigma-Aldrich	S9888
NaF	Sigma-Aldrich	201154
nitrocellulose membrane	Thermo-Scientific	LC2006
NP-40	Thermo-Scientific	85124
Osimertinib	LC Laboratories	O-7200
PBS (10x)	Thermo-Scientific	70011044
Penicillin-Streptomycin Gibco™	Thermo-Scientific	15140122
Phenylmethylsulfonyl fluoride	Sigma-Aldrich	78830
Pierce™ Fast Western Blot Kit	Thermo Scientific	35055
Ponceau S	Merck	1142750010
Power Blotter 1-Step™ Transfer Buffer (5x)	Thermo-Scientific	PB7300
Protease Inhibitor cocktail	Roche	11836170001

RLT lysis buffer	Qiagen	79216
RNase A	Thermo-Scientific	R1253
RNeasy Mini kit	Qiagen	74104
RPMI 1640 Medium	Sigma-Aldrich	R8758
SDS	Sigma-Aldrich	L4509
SOC medium	New England Biolabs	B9020S
Superblock	ScyTek Labs	AAA999
peqGREEN, DNA/RNA Dye	VWR Peqlab	732-3196
T4 Ligase	Thermo-Scientific	46300018
T4 ligation buffer	Thermo-Scientific	46300018
T4 Polynucleotide Kinase (PNK)	New England Biolabs	M0201S
TBS	Carl Roth	1060.1
TEMED	Carl Roth	2367.3
TNF-α	ImmunoTools	12343010
Tris	Carl Roth	5429.2
Tris-Base	Carl Roth	5429.2
Tris-HCL	Carl Roth	9090.3
Trypsin-EDTA	Thermo-Scientific	25200056
Tween-20	Sigma-Aldrich	P2287
Ultratek HRP	ScyTek Labs	ABL008
Viability dye eBioscience	Thermo-Scientific	eF450
Xylazine	Livisto	8-00178
Xylol	Carl Roth	4436.2
β-mercaptoethanol	Carl Roth	4227.3

Table 1: List of Materials

Cell lines and cultivation

EP cells were isolated from $EGFR^{L858R}$ tumors with homozygous p53 knockout from immunocompetent mice after Ad.Cre inhalation. EPA cells were generated by CRISPR-Cas9 knockout of *TNFAIP3* from EP cells by Seungyeon Lim. H1975 LUAD cells, harboring the $EGFR^{L858R}$ and T790M mutations were commercially acquired. All cell lines were cultured in RPMI medium, supplemented with 10% FBS and 1% Penicillin/Streptomycin (P/S) at 37°C and 5% CO_2.

Mice

Mouse experiments were approved by the Austrian Federal Ministry of Science, Research and Economy and followed ethical guidelines (G2:2021-0.746.732) All mice were housed in the animal facility of the Institute of Pharmacology, Medical University of Vienna. Experiments were conducted with intranasal Ad.Cre 8–12-week-old C57BL/6N mice. The experiment involving intratracheal transplantation of tumor cells was conducted on 8–10-week-old B6.Cg-Rag2tm1.1Cgn/J mice.[96]

Intranasal adenovirus inhalation

Mice were anesthetized with a Ketamine/Xylazine solution (Ketamine: 9.43 mg/mL, Xylazine: 1.13 mg/mL in 1x PBS). Each mouse was injected with 250-300 µL of the Ketamine/Xylazine solution according to their body weight (approx. 10 µL/g body weight) subcutaneously into the flank of transgenic C57BL/6N mice. Cre recombinase–expressing adenovirus Ad.CMV-Cre (for EGFR-model) and Ad.SPC-Cre (for KRAS-model) were purchased from the Viral Vector Core of the University of Iowa.[97] Adenovirus with Cre-recombinase (Ad.Cre) was prepared by diluting it in 603 µL DMEM. 6 µL M $CaCl_2$ (7.35 g $CaCl_2$ in 50 mL 1x PBS) were added, and the mixture was placed on ice for 20 min, allowing the virus to form a precipitate with $CaCl_2$. Subsequently the mixture was briefly warmed at 37°C and 50 µL were administered intranasally to each anesthetized mouse. In the KRAS-driven tumor model (Fig. 4) intranasal inhalation of Ad.Cre leads to the transcription of the mutant $KRAS^{G12D}$, knockout of p53 and A20 and the transcription of ovalbumin (OVA). Following the

intranasal inhalation tumors form over time. During this time mice were monitored for symptoms weekly and their body weight was measured every two weeks. At the end of the experiment mice were sacrificed by cervical dislocation. Body weight was measured and lungs and spleens were harvested and weighed.

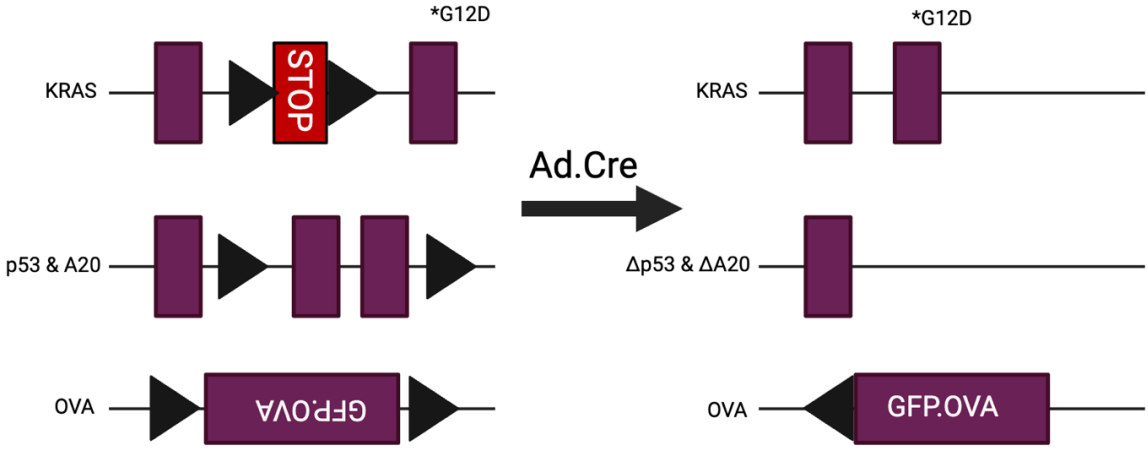

Figure 4: Scheme depicting autochthonous mouse model. Intranasal Ad.Cre inhalation leads $KRAS^{G12D}$, p53- and A20 deficient, OVA expressing lung tumors.

Immunohistochemistry staining

Lungs were harvested, flushed with PBS 1x to remove blood and fixed in 5 mL ROTI® Histofix for 24 hours. The next day the fixed lungs were cut into individual lobes and placed in cassettes and dehydrated in an ascending ethanol concentration (70%, 90%, 96%, 100%) and embedded in paraffin. Paraffin slides were prepared by cutting embedded lungs with a microtome (Dehydration and slide preparation was performed by Michael Machtinger). The paraffin slides were incubated at 60°C for 30 min to melt the paraffin. To dissolve the remaining paraffin the slides were fully submerged in Xylol (3x 10 min.) The lung tissue on the slides was rehydrated by a sequential immersion in ethanol with descending concentrations (100%, 96%, 80%, 70%, 50%) for 30 sec. each, followed by incubation in ddH2O for 5 min. Subsequently antigen retrieval was performed by placing the slides in 1x citrate buffer pH6 or pH9 for 20 or 50 min. (pH and steaming time depends on the antibody used for staining). The slides were cooled for 15 min. and washed 3 times in 1x PBS. Subsequently slides were incubated in H_2O_2 solution (3%) for 15 min. After H2O2 incubation the slides were washed two

times with 1x PBS and once with 1x PBST (1xPBS with 500 µL/L Tween-20). The slides were incubated with Avidin blocking solution at room temperature for 10 min. Slides were washed two times in 1x PBS and once in 1x PBST. The same was repeated with Biotin blocking solution at room temperature for 10 min. and then washed twice with 1x PBS and once in 1x PBST. Afterwards the slides were incubated with Superblock for 7 min. at room temperature for non-specific antibody binding. Slides were washed twice with 1x PBS and once with 1x PBST. Next the slides were incubated with M.O.M.® (Mouse on mouse blocking reagent) for 60 min. at room temperature and washed twice in 1x PBS and once in 1x PBST. After washing the tissue was incubated with the primary antibody over night at 10°C. The following day the slides were washed twice in 1x PBS and once in 1x PBST and incubated with anti-polyvalent biotinylated antibody at room temperature for 10 min, followed by washing twice in 1x PBS and once in 1x PBST. The same step was repeated with Ultratek HRP for 10 min. at room temperature. The staining was developed with Biotin Chromogen for 3-5 min. When the staining was sufficient the reaction was stopped by placing the slides in ddH_2O. The slides were washed three times in ddH_2O, before a counterstaining was performed by submerging the slides in 1:5 diluted hematoxylin for 45 seconds. The slides were washed under running tap water until the remaining hematoxylin was fully removed, and the slides were mounted with Aquatex.

Cell isolation from lungs

Lungs were isolated from mice and placed into 1x PBS until further processing. Each lung was cut into small pieces and incubated with in 5 mL collagenase-DNase solution (1% collagenase, 0.001% DNase in RPMI (10% FBS, 5% P/S) for one hour at 37°C. After incubation the lung pieces were homogenized into a single-cell suspension by filtering through a 70 µm cell strainer. The single cell solution was centrifuged at 300 x g for 5 min. To perform red blood cell lysis the supernatant was removed and the cell pellet was resuspended and incubated in 1 mL Ammonium–chloride–Potassium (ACK) buffer for 5 min at room temperature. To stop the reaction 5 mL RPMI (10% FBS, 1% P/S) were added, and suspension was centrifuged at 300 x g for 5 min. The cell pellets were resuspended in 1x PBS and placed on ice until further processing.

Antibody staining for Flow Cytometry

Cells were washed with 1x PBS and centrifuged for 5 min. at 500 x g at 4°C. After centrifugation supernatant was discarded. Cells were first stained with a viability dye. The viability antibody was diluted 1:2000 in 1x PBS and the cell pellet was resuspended in 1 mL of the viability dye dilution and incubated for 30 min. at 4°C in the dark. To stop the viability staining 2 mL ice cold FACS buffer (2% FBS and 500 nM EDTA into 1x PBS) were added to the cell suspension and centrifuged for 5 min. at 500 x g at 4°C. The supernatant was discarded. Next a FC-blocking solution was prepared by diluting Anti-mouse CD16/32 antibody in ice cold FACS buffer 1:100. Cell pellets were resuspended in 100 µL FC-block dilution and incubated for 30 min. at 4°C in the dark. To stop the FC-blocking 2 mL ice cold FACS buffer were added to the cell suspension and centrifuged for 5 min. at 500 x g at 4°C. The supernatant was discarded. Cells were subsequently stained with different antibodies at different dilutions respectively (Table 2). All antibodies were diluted in FACS buffer, and the antibody staining was performed over night at 4°C.

Antigen	Fluorophore	Company	Product No.
Viability	eF450	eBioscience	65-0863
Anti-mouse CD16/32 (FC-block)	unlabelled	BD Pharmigen	553141
CD45	APC-Cy7	BD Pharmigen	557659
F4/80	APC-R700	BD Pharmigen	565787
CD206	BV-421	Biolegend	141717
CD3	FITC	eBioscience	11003282
CD8	PC7	Biolegend	100721
SIINFEKL-H2-Kb Tetramer chicken ova 257-264	APC	NIH Tetramer Core Facility	58560 (Immune Epitope Database ID (IEDB ID))

Table 2: List of flow cytometry antibody

Cloning for CRISPR-Cas9 plasmid

Figure 5: Plasmid map of pSpCas9(BB)-2A-Puro (PX462) 2.0

Oligo	Sequence
Oligo_hA20 gRNA#6f	CACCGTCAACTGGTGTCGAGAAGTC
Oligo_hA20 gRNA#6f	AAACGACTTCTCCACACCAGTTGAC

Table 3: A20 sgRNA Oligo List

To clone the sgRNA into the pSpCas9(BB)-2A-Puro (PX462) 2.0 vector backbone the leading and lagging sgRNA oligos (Table 3) need to be annealed and phosphorylated. The phosphorylation reaction was prepared according to Table 4.

Reagent	Volume (μL)
Oligo_hA20 gRNA#6f (100 μM)	1
Oligo_hA20 gRNA#6r (100 μM)	1
10x T4 DNA Ligation buffer	1
ddH_2O	6
T4 Polynucleotide Kinase (PNK)	1

Table 4: Oligo ligation mix

The reactions were incubated in a thermo cycler: 37° for 30 min.; 95°C for 5 min.; descending temperature to 25°C at a rate of -5°C per min. Annealed oligos were diluted 1:200 in ddH_2O. To cleave the backbone vector and ligate the annealed oligo duplexes into the CRISPR-Cas9 vector backbone a digestion-ligation mix was prepared according to Table 5.

Reagent	Volume (μL)
pSpCas9 plasmid backbone (100 ng)	X
Oligo duplex (1:200)	2
FastDigest BpiI	1
10x T4 DNA Ligation buffer	2
ddH_2O	X (add up to 20 μL)
T4 Ligase	0.5
Total Volume	20

Table 5: Digestion-ligation mix

The digestion-ligation reaction was incubated in a thermocycler with following program (Table 6)

Temperature	Time	
37°C	5 min	6x
21°C	5 min	

Table 6: Conditions of the digestion-ligation reaction

After polymerase chain reaction (PCR) the PCR product was purified using the FavorPrep™ PCR Clean Up Kit (Favorgen; FAPCK 001-2).

Gel electrophoresis

An agarose gel (2%) was prepared by dissolving 6 g Agarose in 1x Tris-acetate-EDTA (TAE) by heating in the microwave. After letting the gel cool down to ~50°C 6 μL PeqGREEN DNA Gel Stain and the gel was poured into a chamber and let cool until solidified. 6 μL microliters of the Gene Ruler 1kb and 10 μL of PCR products were loaded into the wells of the agarose gel and electrophoresis was run at 120 V for approximately 30 min.

Bacterial Transformation and Plasmid amplification

Competent E. coli DH5α bacteria were thawed on ice. 100 ng of the pSp-Cas9-hA20 plasmid were added to the bacteria and mixed by flicking the microcentrifuge tube carefully and the bacteria were incubated on ice for 30 min. After incubation heat-shock was performed by incubating bacteria at 42°C for 30 sec. Subsequently the bacteria were incubated on ice for 5 min. before adding 500 μL SOC medium and incubating at 37°C under agitation for 1 hour. After incubation 50 - 100 μL of the bacterial suspension were plated on Agarose plates containing ampicillin (100 μg/mL). The Agarose plates were incubated over night at 37°C. The next day single colonies were picked and incubated in 4 mL LB-Medium containing ampicillin (100 μg/mL) over night at 37°C while shaking. The following day Plasmid isolation was performed according to the High Pure Plasmid Isolation Kit.

Transfection and Puromycin selection

H1975 wild type cells were seeded at $1*10^4$ cells per well in 24 well plates and incubated over night at 37°C, 5% CO_2. The transfection was performed with the jetOPTIMUS transfection kit. 0.5 μg of the pSp-Cas9-hA20 plasmid were diluted in 50 μL of jetOPTIMUS buffer, briefly vortexed and spun down. 0.5 μL jetOPTIMUS reagent was added, briefly vortexed, spun down and incubated for 10 min. at room temperature. The transfection mix was added to the respective well dropwise. Cells were incubated with the transfection mix over night at 37°C, 5% CO_2. To confirm a successful transfection a similar plasmid carrying a green fluorescent protein (GFP)

sequence was used as a control. The day after the transfection cells were observed via fluorescence microscopy.

DNA Isolation

Cells were harvested with Trypsin-EDTA and washed in 1x PBS. After centrifugation (300 x g for 5 min. at 4°C) the supernatant was discarded and 200 µL cell lysis buffer (Table 7) and 6 µL RNase A (1 mg/mL) were added to the cell pellet, vortexed briefly and incubated at 55°C at 800 rpm overnight. The following day 85 µL NaCl (M) were added and mixed by inverting the tube 10x followed by centrifugation at 16000 x g for 10 min. The supernatant was transferred into a fresh microcentrifuge tube. 200 µL Isopropanol was added, and the solution was mixed by inversion to precipitate the solved DNA. Following another centrifugation step at 16000 x g for 5 min the supernatant was discarded, and the DNA pellet was washed by adding 1 mL EtOH (70%). The tube was centrifuged again at 16000 x g for 5 min. The supernatant was aspirated as much as possible without disturbing the DNA pellet and the pellet was air dried for approx. 20 min until the remaining supernatant had completely evaporated. Subsequently the DNA pellet was solved in an appropriate volume of ddH_20, depending on the pellet size (20-50 µL). Subsequently the DNA concentration was measured using the Infinite® 200 NanoQuant (Tecan).

Reagent	Concentration
Tris-HCL pH8	50 mM
EDTA	100 mM
NaCl	100 mM
SDS	1%

Table 7: Composition of the cell lysis buffer

Polymerase chain reaction for TIDE sequencing

A PCR reaction mix was prepared according to Table 9 using the primers in Table 8. The PCR was performed according to the program in Table 10.

Primer	Sequence
A20_TIDEseq_f	TTCAGGTGTTGGAGAGCACA
A20_TIDEseq_r	TCACCTAATGGAGGTATGGTGT

Table 8: TIDE-sequencing primers

Reagent	Volume (μL)
GoTaq Buffer 10x	10
A20_TIDEseq_f (10 μM)	2
A20_TIDEseq_r (10 μM)	2
GoTaq G2 DNA Polymerase	0.1
dNTPs (5 mM)	1
DNA (1 μg)	X
H_2O	Up to 50 μL

Table 9: PCR reaction conditions for TIDE-sequencing

Temperature	Time	
95°C	2 min.	
95°C	30 sec.	35x
58°C	40 sec.	
72°C	50 sec.	
72°C	10 min.	
10°C	hold	

Table 10: PCR reaction conditions for TIDE-sequencing

Following the PCR the PCR products were purified with a PCR purification kit (Favorgen; FavorPrep™ GEL/PCR Purification Kit).

Single cell selection

Conditioned cell medium (DMEM, 1 day old, 10% FBS, 5% P/S) was collected and filtered through a 0.22μm sterile filter. Cells were detached from the cell culture dish using Trypsin-EDTA and washed in 1x PBS. After centrifugation (300 x g for 5 min.) the cell pellet was resuspended in complete growth medium (10% FBS, 5% P/S), cells were counted and diluted to a density of 8 cells/mL in the filtered conditioned medium. Using a multichannel pipette 100 μL of the cell suspension were transferred into each Well of two 96 Well plates. The plates were incubated at 37°C, 5% CO_2 overnight. After 1 week the plates were checked for small cell aggregates deriving from a single cell. Single cell colonies were expanded for further analysis. For further characterization DNA of the colonies deriving from the single cells was isolated and used for TIDE sequencing.

Determination of IC_{50}

$3x10^3$ cells were seeded as triplicates per well in a 96 Well plate and cultivated for 6 hours in DMEM (10%FBS, 1% P/S) at 37°C, 5% CO_2. The following day following a serial dilution of osimertinib was prepared according to Table 11.

Dilution	Concentration (μM)
1	50
2	16.6667
3	5.5556
4	1.8519
5	0.6173
6	0.2058
7	0.0686
8	0.0229
9	0.0076
10	0.0025
11	0.0008
12	0

Table 11: Serial dilution of osimertinib

The medium in the 96 well plate was carefully removed and replaced with 100 µL of the respective osimertinib dilution. The cells were treated with osimertinib for 3 days at 37°C, 5% CO_2. Following the treatment the cell viability was measured using the MTT (3-[4,5-dimethylthiazol-2-yl]-2,5 diphenyl tetrazolium bromide) Assay (R&D Systems; 4890-025-K). 10 µL of MTT reagent were added to each well and the plate was incubated for 4h at 37°C, 5% CO_2. Subsequently 100 µL of MTT detergent was added and the plate was incubated over night at 37°C. The next day absorbance of each well was measured at 570nm.

Stimulation and RNA Isolation for RNA-Sequencing

$1x10^5$ cells were seeded per well in a 12 well plate and incubated overnight at 37°C, 5% CO_2. The following day the cells were stimulated with IFN-γ (10 ng/mL), TNF-α (10 ng/mL) and IL-6 (10 ng/mL). Stimulated cells were incubated for 4h at 37°C, 5% CO_2. After incubation the supernatant was aspirated, and the cells were washed with ice cold PBS (1x). 350 µL of RLT lysis buffer (Qiagen; 79216) containing 3.5 µL β-mercaptoethanol was added to each well and incubated for 20 min. After incubation the lysate was transferred to microcentrifuge tubes and frozen at -20°C. The following day RNA was isolated according to the RNeasy Mini kit protocol. On-column DNase I digestion was performed during the isolation protocol. The purified RNA samples were stored at -80°C before they were sent for RNA-sequencing.

RNA Sequencing

Sequencing libraries were prepared from poly(A)-enriched mRNA and sequenced on the Illumina NovaSeq PE150 platform in 150-base pair paired-end mode. RNA sequencing was performed by Biomarker Technologies (BMK) GmbH.

Cell stimulation and RNA Isolation

$2x10^5$ cells were seeded per well in a 12 Well plate and incubated over night at 37°C, 5% CO_2. The following day cells were stimulated with IFN-γ (10ng/mL) for 1h, 4h and 8 hours. Following the stimulation the medium was aspirated, the cells were washed

with PBS (1x) and detached from the surface with Trypsin-EDTA. After cells were fully detached DMEM was added, and the cell suspension was centrifuged at 300 x g for 5 min. and washed in PBS (1x) twice. After centrifugation the supernatant was aspirated, and the RNA was isolated from the cell pellet according to the E.Z.N.A.® Total RNA Kit I protocol. The concentration of the isolated RNA was measured using Infinite®200 NanoQuant (Tecan) and subsequently stored at -80°C.

cDNA Synthesis

cDNA synthesis was performed using the iScript™ cDNA synthesis kit. 384 ng RNA from each sample were used for cDNA synthesis. cDNA reaction mixes were prepared according to Table 12.

Reagent	Volume
RNA	Volume for 384 ng
H_2O	30 µL – RNA volume
5x buffer	8 µL
Reverse transcriptase	2 µL
Total	40 µL

Table 12: cDNA synthesis reaction mix

cDNA synthesis was performed in a thermocycler with the program according to Table 13.

Temperature	Time
25°C	5 min
46°C	20 min
95°C	1 min
4°C	hold

Table 13: Reaction conditions for cDNA synthesis

After cDNA synthesis each sample was diluted 1:10 in nuclease-free H_2O and stored at -20°C.

Real-Time Quantitative PCR

5 µL of the diluted cDNA samples were added to the respective wells of Hard-Shell® 96-Well PCR Plates in triplicates. The plate was kept on a cooling rack while pipetting. For each primer pair a master mix was prepared according to Table 14. Per well 10 µL of master mix were added to the cDNA. Two-step Real-Time Quantitative PCR (RT-qPCR) program (TABLE X) was performed on a CFX Connect™ Thermocycler (Bio-Rad). Analysis was done by calculating the fold change by $2^{-\Delta\Delta Ct}$.

Reagent	Volume
GoTaq® qPCR Master Mix (Promega; A6010)	7.5 µL
Primer mix (fwd. and rev., 10 µM each)	0.75 µL
H_2O	1.75 µL

Table 14: RT-qPCR master mix

RT-qPCR Primers	Sequence
STAT1 f	CCT TCC TGC TGC GGT TCA
STAT1 r	GTT TCT TTC TTC GTG TAG GGT TCA AC
CD274 f	GGC CGA AGT CAT CTG GAC AA
CD274 r	TCT CAG TGT GCT GGT CAC AT

Table 15: RT-qPCR primer list

Temperature	Time	
95°C	30 sec.	
95°C	5 sec.	40x
60°C	30 sec.	
65°C → 95°C in 0.5°C/cycle (Melt curve)		

Table 16: RT-qPCR reaction program

Cell stimulation and protein isolation for Western Blot

$5x10^5$cells were seeded per well in a 6 Well plate and incubated over night at 37°C, 5% CO_2. The following day cells were stimulated with IFN-γ (10ng/mL), TNF-α (10ng/mL) or LPS (10 µg/mL). Following the stimulation the medium was aspirated, the cells were washed with PBS (1x) and detached from the surface with Trypsin-EDTA. After cells were fully detached DMEM was added, and the cell suspension was centrifuged at 300 x g for 5 min. and washed in PBS (1x) twice. After centrifugation the supernatant was aspirated and resuspended in 150 µL Lysis buffer (Table 17) with 1% phenylmethylsulfonyl fluoride and incubated for 10 min on ice and vortexed thoroughly. Subsequently the lysate was centrifuged at full speed (approx. 20000 x g) for 10 min at 4°C. The supernatant was transferred into a pre-cooled microcentrifuge tube and stored at -20°C.

Reagent	Volume	Concentration
Tris pH 7.5 (1 M)	1 mL	20 mM
NaCl (5 M)	1 mL	100 mM
Na_3VO_4 (0.2 M)	0.25 mL	1 mM
NaF (0.5 M)	10 mL	100 mM
Glycerol-2-phosphate (0.2 M)	5 mL	20 mM
EDTA (0.25 M)	0.5 mL	2.5 mM
EGTA (0.25 M)	0.2 mL	1 mM
NP-40	0.5 mL	1%
Protease Inhibitor cocktail tablets	5 tablets	
H_2O	31.55 mL	

Table 17: Composition of cell lysis buffer for protein isolation

Bicinchoninic Acid (BCA) Assay

Protein concentration per sample was determined by Bicinchoninic Acid (BCA) Assay. For the standard curve BSA dilutions were prepared according to Table 18. 25 µL of each BSA standard solution was added into a clear-bottom 96 well plate as duplicates.

From each sample 5 µL were added into the 96 well plate with 20 µL lysis buffer in duplicates. BCA reagent was prepared by diluting Reagent B 1:50 in Reagent A. 200 µL of BCA reagent were transferred into each well containing BSA standard dilutions and samples. The plate was incubated at 37°C for 30 min before measuring absorbance at 562 nm wavelength using the Infinite® 200 NanoQuant (Tecan). The absorbance values of the BSA standards were used to create a standard curve. The standard curve was used to calculate the protein concentration of each sample.

Vial	Volume of BSA	Volume of diluent (Lysis buffer) (µL)	Final BSA concentration (µg/mL)
1	300 (of 2 mg/mL Stock)	0	2000
2	300 (of 2 mg/mL Stock)	100	1500
3	300 (of 2 mg/mL Stock)	300	1000
4	300 of vial 3	300	500
5	300 of vial 4	300	250
6	300 of vial 5	300	125
7	300 of vial 6	400	25
8 (Blank)	0	400	0

Table 18: BSA dilutions for BCA standard curve

SDS-PAGE and Western Blot

Reagents	Mass / Volume
Running buffer (TGS) (10x)	
Tris-Base (121.1 g/mol)	30.3 g (→ 0.25 M)
Glycine (75.1 g/mol)	144.4 g (→ 1.92 M)
SDS (288.4 g/mol))	10 g (→0.035 M)
TBS (10x)	
Tris-Base (121.1 g/mol)	24 g
Tris-HCl (158.6 g/mol)	5.6 g
NaCl (58.4 g/mol)	88 g
ddH_2O	Up to 1000 mL
TBS-T (1x)	

TBS (10x)	100 mL
ddH_2O	899 mL
Tween-20	1 mL
Blocking Solution	
TBS-T (1x)	100 mL
BSA	5 g
Ponceau solution	
Ponceau S (760.57 g/mol)	5 g (→ 1.3 mM)
Acetic acid (anhydrous)	25 mL (→ 5%)
ddH_2O	475 mL
Stripping buffer	
Glycine	15 g
SDS	1 g
Tween-20	10 mL
ddH_2O	980 mL
	→ adjust to pH 2.2

Table 19: List of reagents and solution for western blot

Reagent	Volume (mL) per gel	
	Separating Gel (8%)	Stacking Gel (5%)
ddH2O	4.6	3.9
Acrylamide/Bis-acrylamide (30%)	2.7	0.67
1.5 M Tris (pH 8.8)	2.5	-
1.5 M Tris (pH 6.8)	-	0.5
10% SDS	0.1	0.04
10% APS	0.1	0.04
TEMED	0.008	0.003
Total	10	4

Table 20: Preparation of separation and stacking gels for SDS-PAGE

	Target protein	Company, Cat. No	Dilution
Primary Antibodies	A20	Santa Cruz Biotechnology, sc-166692	1:2000
	pSTAT1(Y701)	Cell signaling technology, 58D6	1:1000
	STAT1	Cell signaling technology, 9H2	1:1000
	pSTAT3(Y705)	Cell signaling technology, D3A7	1:2000
	STAT3	Cell signaling technology, 124H6	1:1000
	HSP70	Santa Cruz Biotechnology, sc-24	1:3000
Secondary Antibodies	Anti-mouse IgG, HRP-linked Antibody	Cell Signaling Technology, 7076	1:3000
	Anti-rabbit IgG, HRP-linked Antibody	Cell Signaling Technology, 7074	1:3000

Table 21: Western blot antibody list

Separating gel (8%) and Stacking gel (5%) were prepared according to Table 20. For each sample 30 µg of protein was used and diluted to a final volume of 30 µL in lysis buffer. 6 µL of Laemmli buffer (6x) were added to each sample and incubated at 95°C for 5 min and loaded on the SDS-Gel. The gel was run at constant voltage 60V for 20 min. and 120V for approximately 90 additional minutes. After running the gel semi-dry blotting was performed to transfer the proteins onto a nitrocellulose membrane Power Blotter 1-Step™ Transfer Buffer (5x) was diluted 1:5 in ddH_2O. Filter papers and one

membrane were equilibrated in pre-diluted 1x Power-blotter solution. Per SDS-Gel 4 sheets of filter paper and one membrane were stacked onto the Power Blotter–Semi-dry Transfer System (Thermo-Scientific). Blotting was performed for 12.5 min at 25V. After blotting the membrane was stained with Ponceau S solution to verify the successful transfer. To reverse the Ponceau S staining the membrane was washed 3x in TBS-T (Table 19). After de-staining the membrane was incubated in blocking solution (Table 19) under agitation for 1h at room temperature. The primary antibody was diluted according to Table 21 in blocking solution. The membrane was incubated in the antibody dilution overnight at 4°C under agitation. The next day the membrane was washed 3x for 5 min. in TBS-T before diluting the secondary antibody to in blocking solution and adding it to the membrane (Table 21). The membrane was incubated for 1h at room temperature under agitation with the secondary antibody solution. Subsequently the membrane was washed 3x for 5 min. in TBS-T. For detection the Pierce™ Fast Western Blot Kit was used by mixing reagent A with reagent B in a ratio of 1:50. After detection the membrane was stripped by incubating in stripping buffer (Table 19) for 30-40 min at 37°C. Following the stripping the membranes were washed 3x in TBS-T for 5 min. before incubation in blocking solution for 1h at room temperature. After blocking the membrane could be used for incubation with another primary antibody.

IFN-γ treatment for flow cytometry

Cells were treated with 1 µg/mL Doxycycline (DOX) in DMEM for three days before seeding $5x10^4$ cells per well in a 12 Well plate and incubation over night at 37°C, 5% CO2 in DMEM (+ DOX 1 µg/m). The cells were treated for 1, 2, or 3 days with IFN-γ (5 ng/mL) before harvesting by trypsinising, and washing the cell pellet after centrifugation (300 x g, 5 min., 4°C) twice with ice cold PBS (1x). After centrifugation the supernatant was discarded, and the cells were stained with viability dye. The viability dye was diluted 1:2000 in 1x PBS and the cell pellet was resuspended in 1 mL of the viability antibody dilution and incubated for 30 min. at 4°C in the dark. To stop the viability staining 2 mL ice cold FACS buffer (2% FBS and 500 nM EDTA in 1x PBS) were added to the cell suspension and centrifuged for 5 min. at 500 x g at 4°C. The supernatant was discarded. Cells were subsequently stained with different antibodies

at different dilutions respectively (Table 22). All antibodies were diluted in FACS buffer, and the antibody staining was performed for 30 min. at 4°C.

Antigen	Fluorophore	Company	Product No.	Dilution
Viability	eF450	eBioscience	65-0863	1:2000
MHC1	APC	BioLegend	111513	1:200
PD-L1	BV-421	BioLegend	124315	1:200

Table 22: List of flow cytometry antibodies

Statistical analysis

Data is presented as means ± standard error of the mean (SEM). Student's t test was used to compare two groups for well-distributed samples. Analysis of variance (ANOVA) test was conducted to compare variances across means of more than two groups. For Kaplan-Meier survival analysis, log-rank test was used. Student's t test, ANOVA and log-rank tests were performed using GraphPad Prism 10.3.1. Gene set enrichment analysis (GSEA) was performed using the GSEA_4.3.3 software (UC San Diego and Broad Institute).[98,99] RNA-Seq data were normalized using the DESeq2 package,[100] and variance-stabilizing transformation (VST) was applied. Both steps were conducted in RStudio. Multiple unpaired Student's t data were performed on the RNA-Seq. data followed by Benjamini-Hochberg correction using the statsmodels.stats.multitest module in Python 3.9. P-values < 0.05 were considered non-significant (ns). P-values ≤ 0.05 were considered statistically significant. Significance was annotated by asterisk: *P ≤ 0.05; **P ≤ 0.01; ***P ≤ 0.001; ****P ≤ 0.0001.

Correction Tools

ChatGPT-4 (OpenAI) was used for grammar and spelling corrections, as well as occasional rephrasing for improved readability.

Results

A20 knockout increases inflammatory response signaling

To assess whether loss of A20 leads to a differential pathway expression in EGFR-mutant cancer cells as in KRAS-mutant cancer cells, we performed RNA-sequencing followed by gene set enrichment analysis (GSEA) on $KRAS^{G12D}$:Δp53 (KP) and $KRAS^{G12D}$:Δp53:ΔA20 (KPA) cells (Fig. 6). We compared these to their EGFR-mutant counterparts (EP, EPA). KP and EP tumor cells were previously isolated from tumor-bearing C57BL/6 mice and A20-deficient EPA and KPA cells were generated by CRISPR-Cas9 knockout. GSEA revealed an upregulation of inflammatory pathways in A20-deficient cell lines (KPA, EPA) compared to A20-proficient cells (KP, EP). Notably both KPA and EPA showed an upregulation in inflammatory and immune-related pathways, such as inflammatory response, IFN-γ and IFN-α response, all well described features of A20 as it negatively regulates NF-κB-mediated inflammatory response.

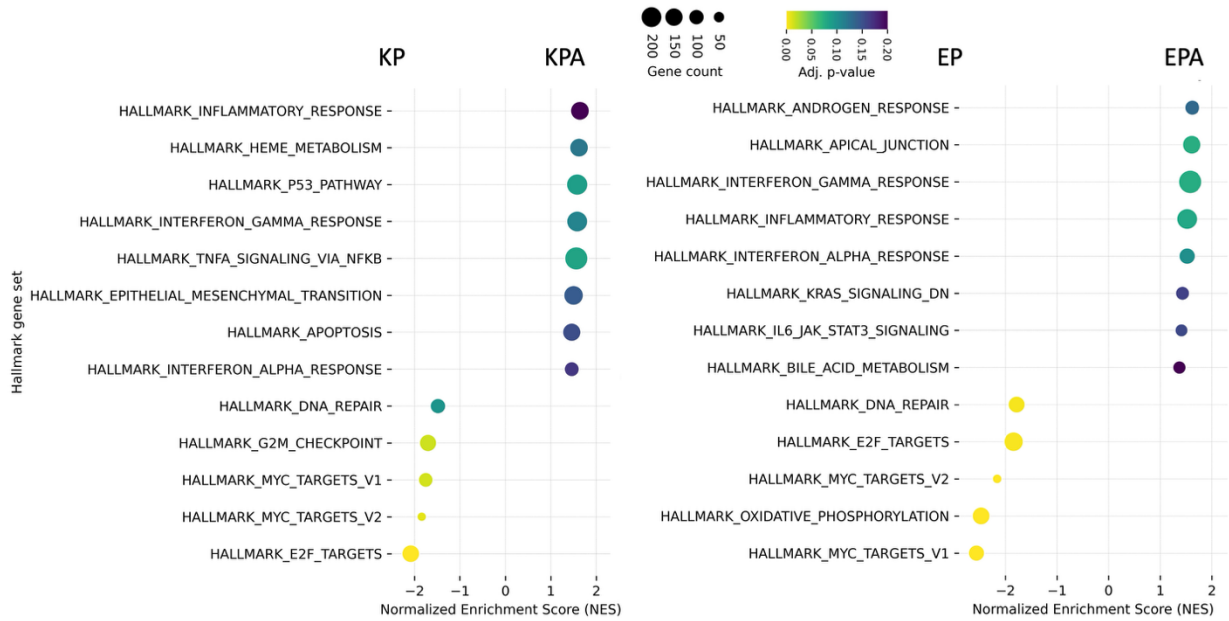

Figure 6: Gene set enrichment analysis of $KRAS^{G12D}$:Δp53 (KP) vs $KRAS^{G12D}$:Δp53:ΔA20 (KPA) and $EGFR^{L858R}$:Δp53 (EP) vs $EGFR^{L858R}$:Δp53:ΔA20 (EPA) cells, analyzed by RNA-seq. Bubble plots show enriched hallmark gene sets (Molecular Signatures Database; MSigDB). The x-axis indicates the Normalized enrichment score (NES). The bubble size correlates to the number of genes in each gene set. The bubble color indicates the adjusted p-value.

Furthermore, some of the most significantly downregulated pathways in both, KRAS- and EGFR-mutant cells upon loss of A20, include pathways related to cell proliferation, such as Myc targets V1/V2, DNA-repair and E2F-targets, suggesting that loss of A20 not only affects the inflammatory response of cells, but may also influence cell proliferation. Additionally, no gene sets that were enriched in one group were downregulated in the other, suggesting that loss of A20 leads to the enrichment and downregulation of similar pathways, in both KRAS- and EGFR-mutant LUAD cells.

A20 acts as an oncogene and alters immune cell infiltration in OVA-expressing KRAS-mutant tumors

In KRAS-mutant lung tumors A20 was shown to influence immune cell infiltration, notably a decrease of $CD3^+$ T cell and an increase of $F4/80^+$ macrophages[86]. To determine whether the incorporation of OVA in the autochthonous mouse model altered the immune infiltrate in KRAS-mutant tumors we administered adenovirus encoding Cre-recombinase (Ad.Cre) in genetically engineered C57BL/6 mice, leading to the development of KPO ($KRAS^{G12D}$: Δp53:OVA) and KPOA ($KRAS^{G12D}$:Δp53:ΔA20:OVA) tumors (Fig. 4). 14 weeks after tumor initiation, lungs of KPOA tumor bearing mice showed a significantly higher tumor burden (Fig. 7A), consistent with the previously described lower survival of KPOA-tumor bearing mice. To assess the tumor infiltration of immune cells immunohistochemistry (IHC) was performed. IHC revealed a decrease of $CD3^+$ T cells (Fig. 7B) and an increase of $F4/80^+$ macrophages (Fig. 7C) within the TME KPOA tumors, 14 weeks post tumor initiation. These results are in line with the previously described tumor burden and infiltration of non-immunogenic (OVA-deficient) KRAS-mutant tumors described in *Breitenecker et al.,* supporting the notion that OVA expression does not alter the dynamics in KRAS-mutant LUAD.[86] The observed differences in survival, tumor burden, and immune cell infiltration between KPO and KPOA can therefore be attributed to the loss of A20.

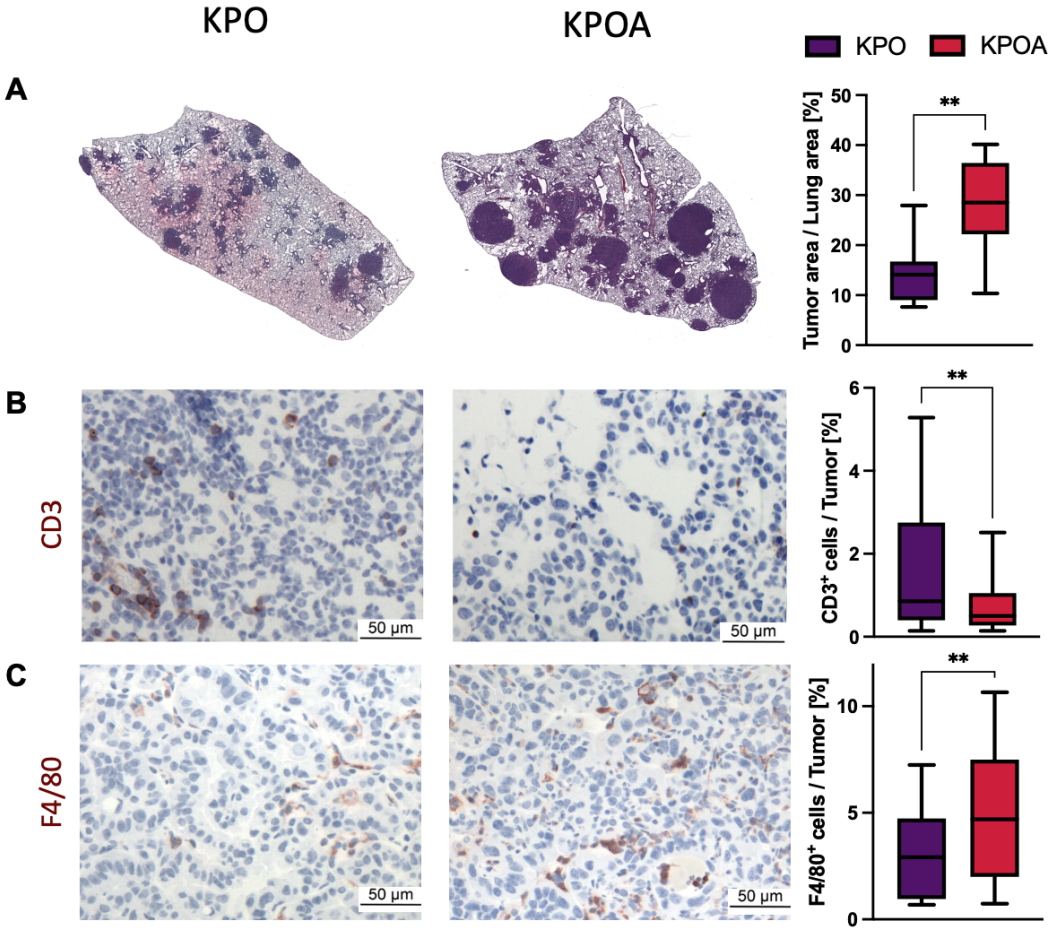

Figure 7: (A) Tumor burden analysis of mice bearing KRAS^{G12D}:Δp53:OVA (KPO) vs KRAS^{G12D}:Δp53:ΔA20:OVA (KPOA) tumors 14 weeks post tumor initiation. Images show representative H&E-stained lung sections. Graph shows the ratio between the tumor area and total lung area in %. **(B)** IHC analysis of CD3 staining. Images show representative tumor regions. Graph shows the percentage of CD3$^+$ cells per tumor 14 weeks post tumor initiation. **(C)** IHC analysis of F4/80 staining. Images show representative tumor regions. Graph shows the percentage of F4/80$^+$ cells per tumor 14 weeks post tumor initiation. **P < 0.01

Loss of A20 does not impact early tumor development

To investigate the role of A20 in EGFR-mutant LUAD, an autochthonous mouse model was established by crossing TetO-EGFR^{L858R} mice with Lox-Stop-Lox-tTA mice, combining the Tet-off system with the LoxP recombination model. Upon inhalation of Ad.Cre, the LoxP-Stop-LoxP cassette is excised in infected lung epithelial cells. This site-specific recombination leads to the expression of tetracycline-controlled transactivator (tTA) which subsequently binds to the Tet operator sequences (TetO). Binding of tTA to TetO activates the transcription of EGFR with the cancer-inducing L858R mutation. Furthermore LoxP-driven recombination leads to the deletion of *Tp53* and *Tnfaip3*, leading to a knock-out of p53 and A20 (Fig. 8A).

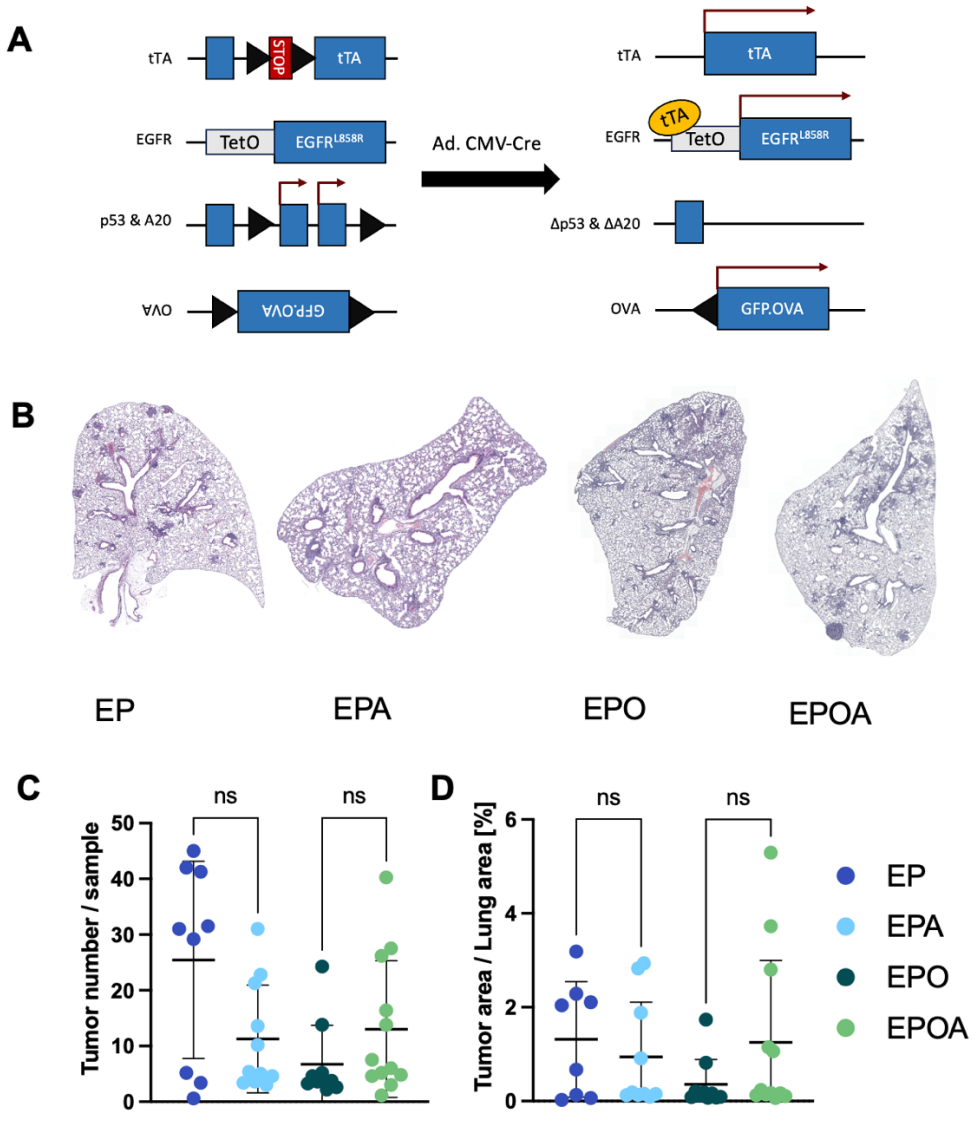

Figure 8: (A) Scheme depicting autochthonous mouse model. Intranasal Ad.Cre inhalation leads $EGFR^{L858R}$, p53- and A20 deficient, OVA expressing lung tumors. **(B)** Representative H&E-stained lung sections for each group. **(C)** Total number if tumors per analyzed sample. **(D)** Ratio between the tumor area and total lung area in %. ns = not significant, determined by one-way ANOVA.

This model was used to induce tumorigenesis of EP, EPA, EPO and EPOA tumors in C57BL/6 mice. Preliminary data showed a significant reduction in tumor burden after 18 weeks (Fig. 3E, 3F), corresponding to increased survival of mice (Fig. 3D) with EPOA tumors. To assess tumor development over time, tumor burden was analyzed 11 weeks post tumor initiation. After 11 weeks, tumors remained small across all groups (Fig. 8B). Lungs with EP tumors showed a slightly higher tumor number than lungs with EPA tumors and lungs with EPOA tumors showed a tendency of a higher tumor number than EPO tumors, however these differences were not significant

(Fig. 8C). EPOA tumors also tended to have a slightly higher tumor to lung area ratio, but also in this case the difference was not significant (Fig. 8D).

Loss of A20 decreases T cell number and increases macrophage number in early-stage EGFR-mutant tumor-bearing lungs

Next, we investigated how A20 impacts the composition of the TME. Lungs of EPO and EPOA tumor-bearing mice were isolated and processed into a single-cell suspension 11 weeks after tumor initiation. The isolated cells were stained for common immune cell markers and analyzed by flow cytometry. Lungs with EPOA tumors exhibited a decrease in total T cell number ($CD3^+$) and an increase in macrophage number ($F4/80^+$) upon loss of A20 (Fig. 9A). Even though a decrease in total T cells could be detected, no significant change in the number of $CD8^+$ T cells were observed (Fig. 9B). To confirm whether the $CD8^+$ T cells within the lungs were tumor-specific, we used a SIINFEKL tetramer to detect OVA-specific $CD8^+$ T cells (TET^+). In both EPO and EPOA samples tumor-specific $CD8^+$ T cells were detected, however their abundance did not differ between groups (Fig. 9C). To assess macrophage polarization, we stained for CD86, typically associated with M1 macrophages, and CD206, a marker of tumor-promoting M2 macrophages.

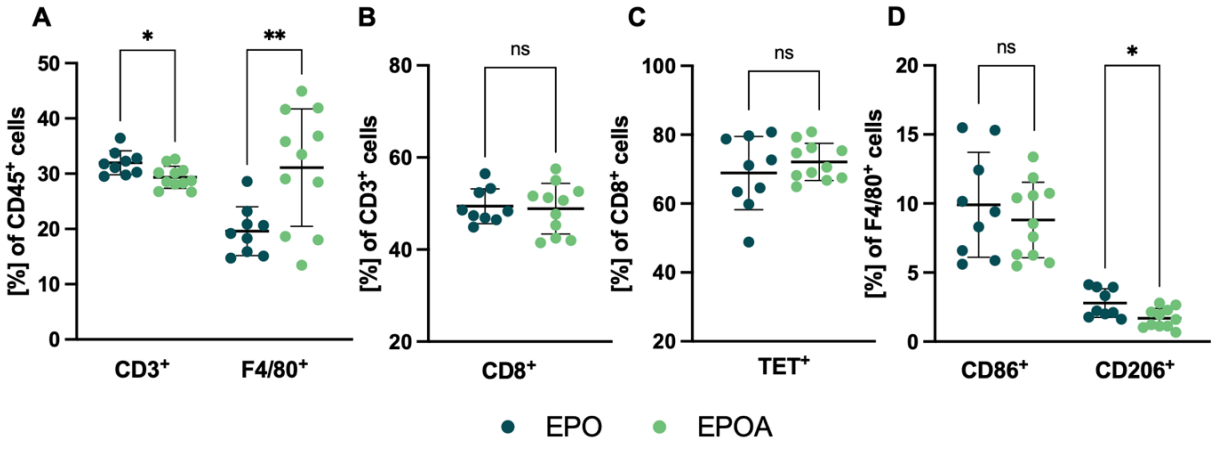

Figure 9: (A) Percentage of T cell ($CD3^+$) and macrophage ($F4/80^+$) populations of total live immune cells ($CD45^+$) detected by flow cytometry in single-cell suspension from isolated, EPO and EPOA tumor-bearing mouse lungs. **(B)** Percentage of $CD8^+$ T cells of total T cells ($CD3^+$). **(C)** Percentage of OVA-specific T cells (TET^+) of total $CD8^+$ T cells. **(D)** Percentage of M1 ($CD86^+$) and M2 ($CD206^+$) macrophages of total macrophages (F4/80). ns = not significant, *P < 0.05, **P < 0.01.

We did not detect a significant difference in M1 macrophage number, however lungs with EPOA tumors demonstrated a lower number of M2 polarized macrophages (Fig. 9D). Notably, $CD206^+$ macrophages constituted a very small fraction of total macrophage number ($F4/80^+$), accounting for less than 5% of total macrophages.

A20 deficiency leads to increased T cell number and decreased macrophage number in the tumor microenvironment over time

Since flow cytometry analysis of the whole lung reflects the relative abundance of specific immune cell populations within the entire lung rather than specifically in the TME, IHC analysis was performed 11 weeks after tumor initiation to directly assess immune cell infiltration in the tumors. Tumors were stained for $CD4^+$ T cells, $CD8^+$ T cells, $F4/80^+$ macrophages and $CD206^+$ macrophages. The percentage of positive cells was quantified per tumor. IHC analysis revealed no significant differences in $CD4^+$ T cell infiltration between EPO and EPOA tumors (Fig. 10A). However, EPOA tumors exhibited a significant reduction in CD8+ T cell infiltration compared to EPO tumors (Fig. 10B), suggesting that loss of A20 leads to an impaired recruitment of $CD8^+$T cells. In contrast, $F4/80^+$ macrophage infiltration was not affected by the loss of A20 (Fig. 10C). Similarly, the abundance of $CD206^+$ M2-like macrophages was comparable between EPO and EPOA tumors (Fig. 10D). To assess changes in the TME upon loss of A20 at a later stage during tumor progression, the immunohistochemical analysis was also performed 18 weeks after tumor initiation. Quantification of $CD4^+$ T cells revealed a significant increase of helper T cells in the TME of EPOA tumors compared to EPO tumors (Fig. 11A). Similarly, a higher $CD8^+$ T cell infiltration was observed in EPOA tumors (Fig 11B). In contrast, staining for $F4/80^+$ macrophages (Fig. 11C) and $CD206^+$ M2-like macrophages (Fig. 11D) revealed a significant decrease of these immune cell populations in EPOA tumors compared to EPO tumors. These results indicate that loss of A20 enhances T cell infiltration but reduces macrophage infiltration in the TME during advanced tumorigenesis.

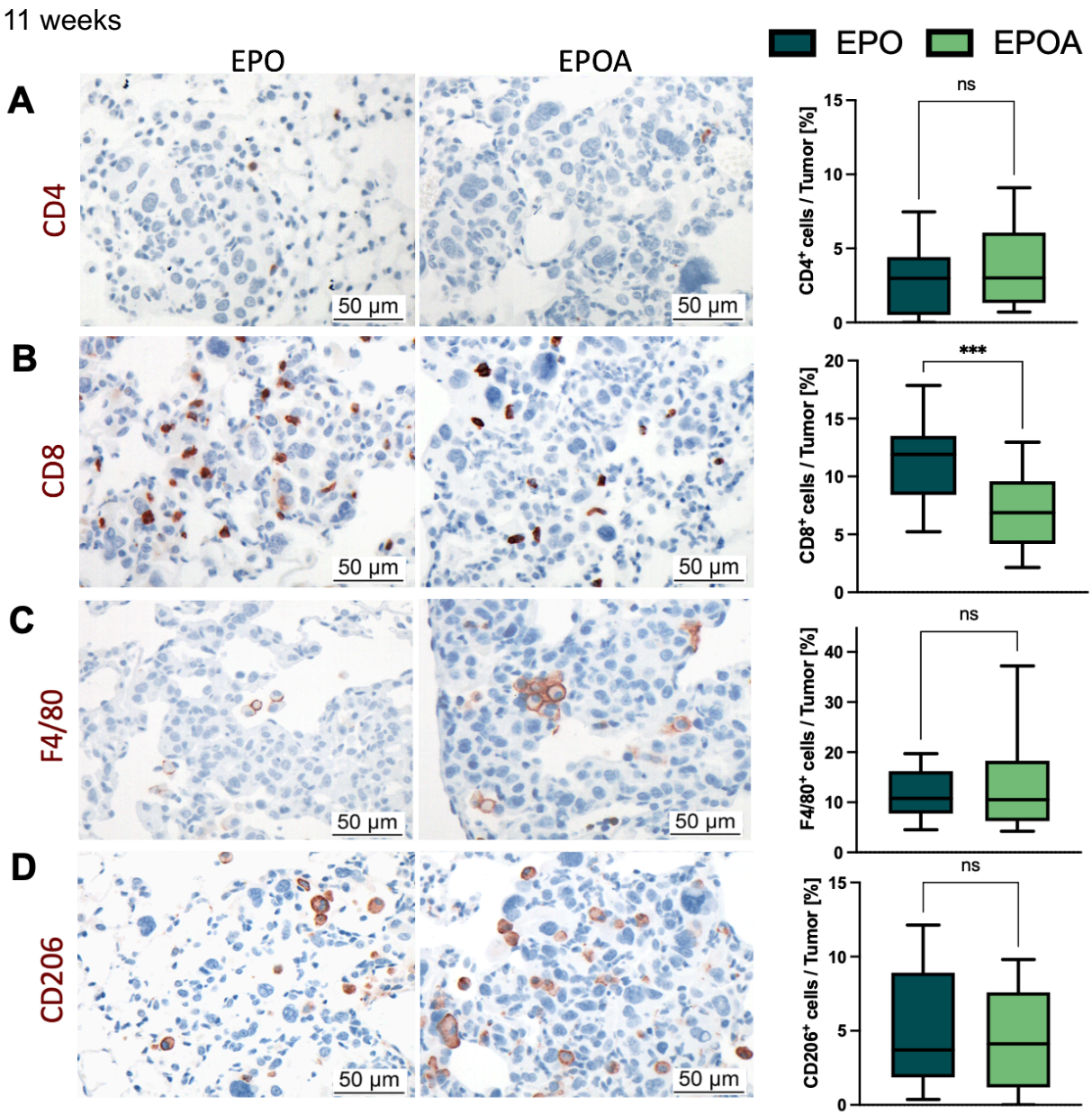

Figure 10: Representative immunohistochemical stainings for **(A)** $CD4^+$, **(B)** $CD8^+$, **(C)** $F4/80^+$ and **(D)** $CD206^+$ cell infiltration in lung sections of EPO and EPOA tumor bearing mice, harvested 11 weeks after Ad.Cre-mediated tumor initiation. Box plots represent the quantification of the indicated immune cell populations within individual tumors 11 weeks post tumor initiation. Boxes denote 25th and 75th percentiles, whiskers denote the 10th and 90th percentiles. ns = not significant, ***P < 0.001.

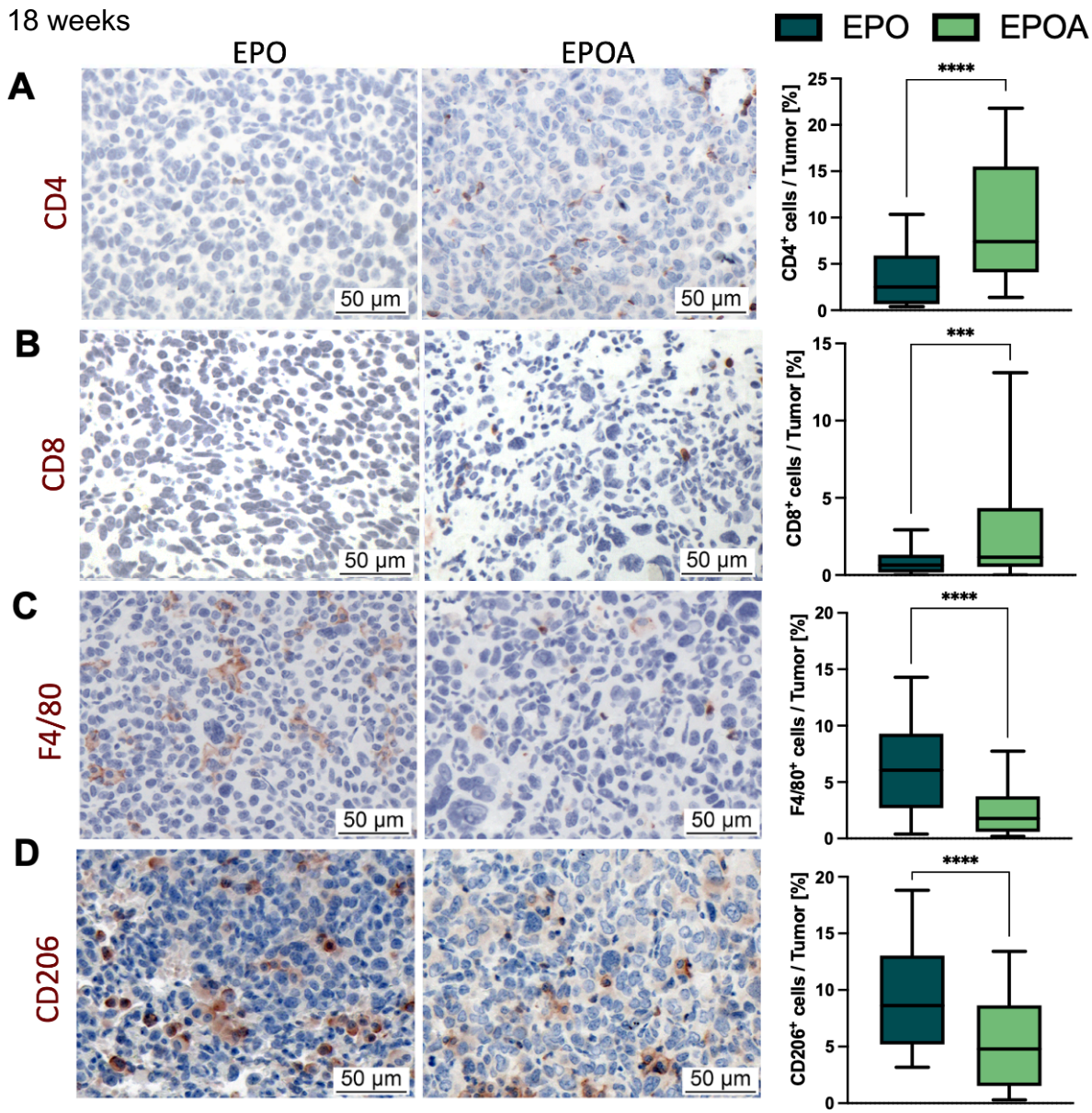

Figure 11: Representative immunohistochemical stainings for **(A)** $CD4^+$, **(B)** $CD8^+$, **(C)** $F4/80^+$ and **(D)** $CD206^+$ cell infiltration in lung sections of EPO and EPOA tumor bearing mice, harvested 11 weeks after Ad.Cre-mediated tumor initiation. Box plots represent the quantification of the indicated immune cell populations within individual tumors 18 weeks post tumor initiation. Boxes denote 25^{th} and 75^{th} percentiles, whiskers denote the 10th and 90th percentiles. ***P < 0.001, ****P < 0.0001.

Enhanced tumor progression of A20-deficient tumors in T cell–deficient Rag2$^{-/-}$ mice

The increased T cell infiltration observed in EPOA tumors suggests that T cells play a critical role in restricting tumor growth in the absence of A20. To investigate the role of T cells we used Rag2$^{-/-}$ mice, which lack mature B cells and T cells. We performed orthotopic, intratracheal transplantation to engraft EP and EPA cells in the lung tissue and harvested the lungs after 10 weeks. During this time the body weight of the mice was monitored weekly, since with developing lung tumors eventually lose body weight. Mice with EP and EPA tumors stopped gaining body weight 7 weeks after transplantation and some mice started losing body within weeks 9 and 10. The body weight changes in mice with EP and EPA tumors were comparable over the 10 weeks (Fig. 12A). At the endpoint of the experiment however EPA tumor-bearing mice exhibited significantly heavier harvested lungs and an increased lung to body-weight ratio (Fig. 12B). Lungs with EPA tumors visually showed a significant increase in tumor number and tumor size (Fig. 12C). This was confirmed by tumor burden analysis, where EPA tumors exhibited a significantly increased tumor area to lung area ratio (Fig. 12D).

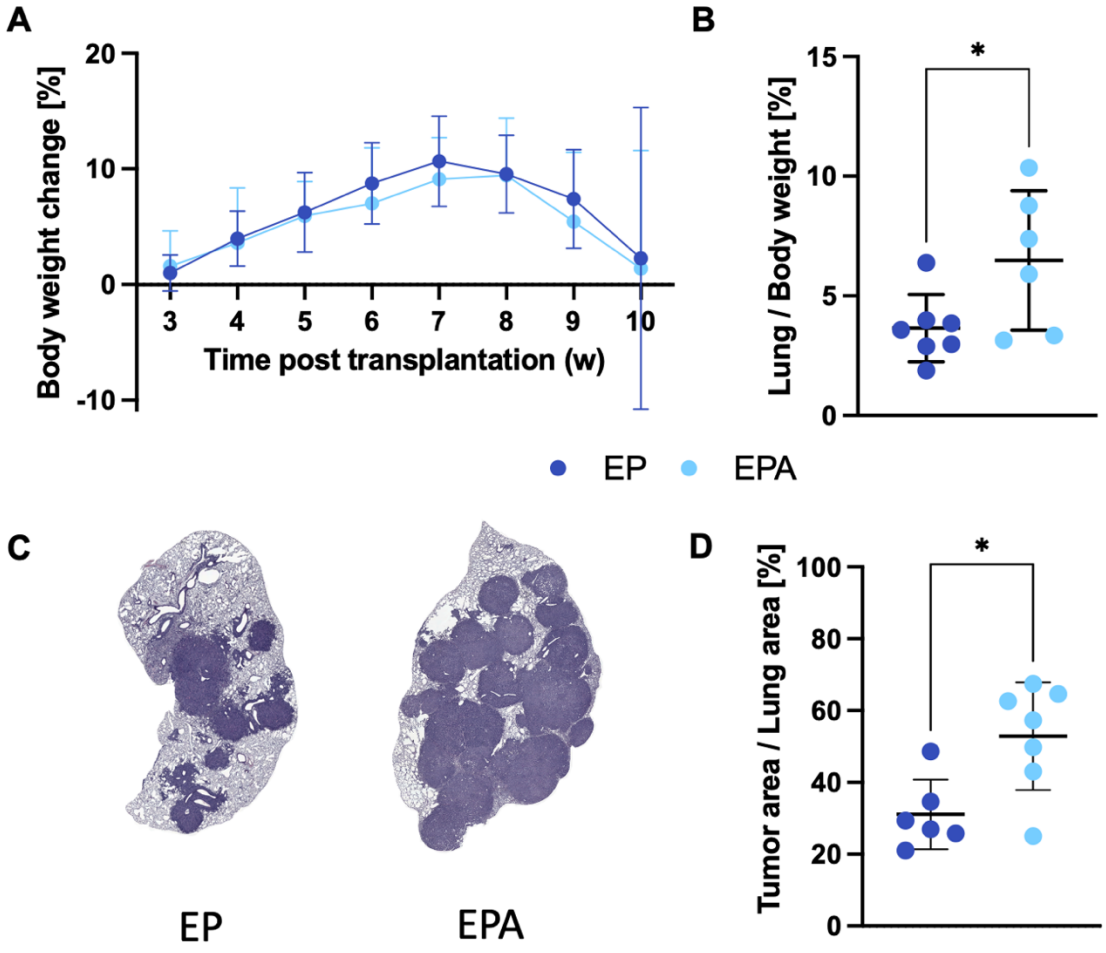

Figure 12: (A) Relative body weight change of mice with EP and EPA lung tumors in weeks after intratracheal transplantation. **(B)** Ratio between the lung and body weight of mice with EP and EPA lung tumors in %. **(C)** Representative pictures of EP and EPA tumor-bearing lungs. **(D)** Ratio between the tumor area and total lung area of lungs with EP and EPA tumors. *P < 0.05, **P < 0.01.

A20 deficiency enhances expression of genes involved in T Cell recruitment and activation

To determine how loss of A20 contributes to an increased T cell infiltration in the TME, we determined genes involved in T cell migration, activation and immune modulation, that are part of gene sets enriched in A20-deficient LUAD cells (Fig. 13A). Additionally, we included IL-15, CD274 and CD276 in the following analysis, since these genes are also known to play key roles in T cell activation and function.[101–103] RNA-Seq-based gene expression data of genes involved in T cell migration, activation and immune modulation was analyzed for differential expression in EP vs EPA cells (Fig. 13B). Cells

were stimulated with immune stimuli (IFN-γ (10 ng/mL), TNF-α (10 ng/mL), IL-6 (10 ng/mL)) for 4 hours to mimic an inflammatory microenvironment. No significant changes could be observed in Stat1 or Stat3 expression, however Jak2 expression was upregulated in EPA cells. This indicates that a loss of A20 does not directly alter Stat1 and Stat3 mRNA levels but may influence STAT1 and STAT3 pathway activation via increased Jak2 expression, as JAK2 phosphorylates both transcription factors.[104] Transcription of Cxcl10 and Il15, both associated with regulation of T cell activity were upregulated in EPA cell compared to EP cells. No significant difference in expression of the chemokines Cxcl9 and Cxcl11 was detected. Furthermore, no differential expression was observed in Transporter associated with antigen processing-1 (Tap1) and -2 (Tap2), which both play important roles in in the MHC class antigen processing machinery.[105] To assess whether loss of A20 alters expression of cell adhesion molecules, differential expression of Intercellular adhesion molecule 1 (Icam1) and Vascular cell adhesion molecule 1 (Vcam1) was investigated. Both adhesion molecules were significantly upregulated in EPA cells. Finally, expression analysis of immune checkpoint molecules revealed no significant difference in Cluster of differentiation 274 (Cd274, encoding PD-L1) expression and an upregulation of Cd276 (encoding B7-H3) expression in EPA cells. To investigate the expression levels of PD-L1 and MHC1 on the surface of EP and EPA tumor cells we stained for both molecules after stimulating EP and EPA tumor cells with IFN-γ (10 ng/mL) for 72 hours and analyzed expression levels using flow cytometry. We observed a slight increase of both PD-L1 and MHC1 expression in EPA cells, compared to EP cells (Fig. 13C).

Next, we investigated whether there were significant differences in the expression of these genes of interests between EPA and KPA cells (Fig. 13D), since in KPA cells, the opposite phenotype was observed *in vivo*: a reduced T cell infiltration within the TME upon loss of A20. Stat1 and Stat3 expression levels were both elevated in EPA cells, compared to KPA cells, whereas expression of Jak2 was higher in KPA cells. Among the chemokines analyzed, expression of Cxcl10 was significantly upregulated in EPA cells. Expression of Cxcl9, Cxcl11 and Il15 remained unchanged. Furthermore, Tap1 expression was increased in EPA cells, whereas Tap2 expression did not differ significantly between the two groups. Expression of Icam1 remained consistent between the groups, while Vcam1 was significantly higher in KPA cells. expression of

the immune checkpoint molecule Cd274 (PD-L1) was elevated in KPA cells, whereas Cd276 (B7-H3) was expressed at higher levels in EPA cells.

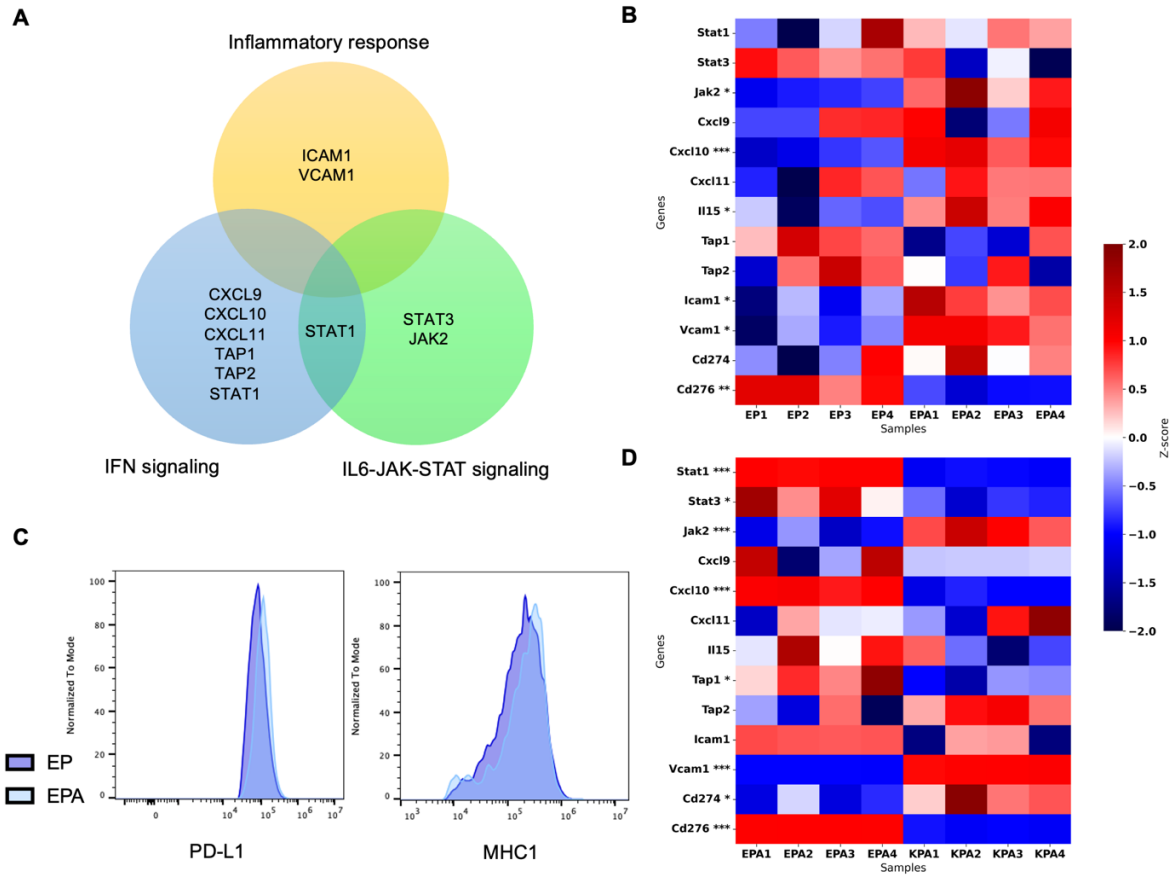

Figure 13: (**A)** Venn diagram of genes involved in T cell recruitment and activation found in upregulated hallmark pathways in EPA and KPA cells. Heatmap of RNA-Seq-based gene expression of genes involved in T cell migration and activation or immune regulation in **(B)** EP (n=4) vs EPA (n=4) and **(D)** EPA (n=4) vs KPA (n=4) tumor cells after stimulation with IFN-γ (10 ng/mL), TNF-α (10 ng/mL) and Il-6 (10 ng/mL). RNA-Seq data were normalized using DESeq2 with variance-stabilizing transformation (VST). Gene-wise z-score normalization was subsequently applied across samples to standardize expression for heatmap visualization. A higher z-score corresponds to a higher gene expression relative to the mean across samples. Outliers were determined by Grubbs' test and replaced with the group mean to improve heatmap visualization. Asterisks next to the gene symbol indicate statistical significance as determined by student's t-test (Outliers were excluded in statistical analysis). *P < 0.05, **P < 0.01. **(C)** Histogram of flow-cytometry analysis of PD-L1 and MHC1 expression after 72h of IFN-γ stimulation (10 ng/mL).

Generation and Validation of A20 Knockout in EGFR-Mutant H1975 Cells

To assess whether loss of A20 also affects other EGFR-driven LUAD cell lines we used CRISPR-Cas9 to create an A20-knockout H1975 cell line. H1975 cells are a well-established model for EGFR-mutant LUAD. The A20 knockout was validated by Sanger-sequencing and Tracking of Indels by Decomposition (TIDE) analysis and western Blot. TIDE analysis revealed a +1 insertion in 28.2% of alleles, a -1 deletion in 24.1% of alleles and a -9 deletion in 21.7% of alleles (Fig. 14A). The -9 deletion is an in-frame deletion, potentially leading to the expression of a truncated A20 protein. However, western blot analysis revealed that A20 expression was absent in H1975-ΔA20, even after stimulation with TNF-α or LPS, to induce expression of A20 via NF-κB signaling. In contrast, A20 expression could be detected in H1975-WT cells (Fig. 14B).

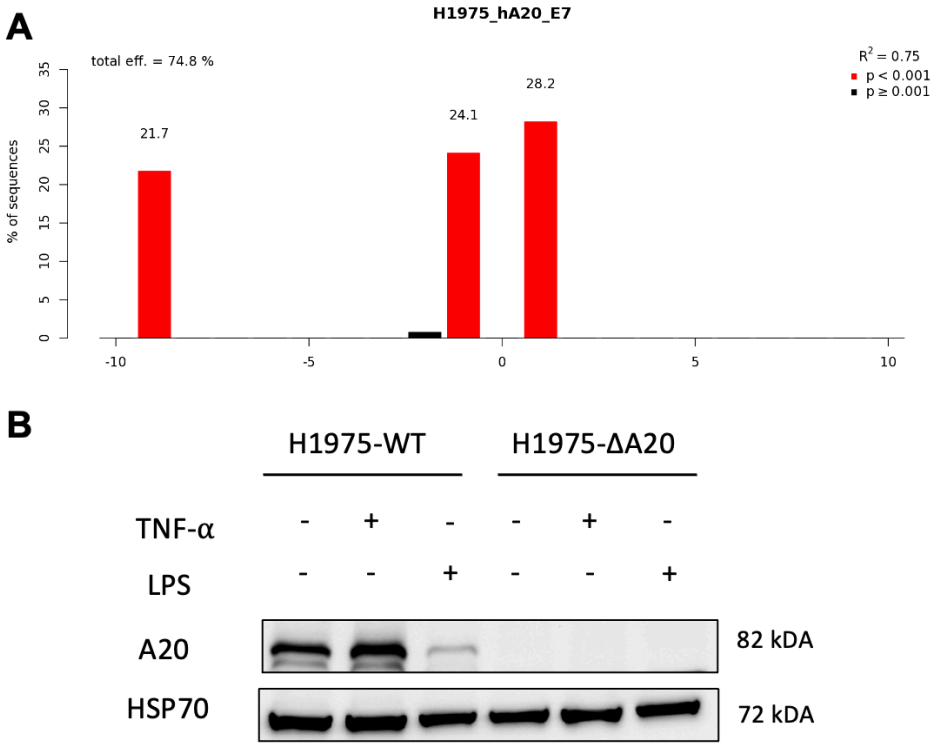

Figure 14: (A) Indel spectrum and its total efficiency of the CRISPR-Cas9 generated H1975-ΔA20 cell line, compared to H1975 WT cells. **(B)** Western Blot of A20 expression in H1975-WT and H1975 after stimulation with TNF-α (10 ng/mL) and LPS (1 ng/mL) for 24h. Heat Shock Protein 70 (HSP70) was used as a housekeeping control.

Loss of A20 enhances STAT1 signaling and alters proliferation and drug sensitivity in EGFR-Mutant LUAD Cells

In murine isolated EP and EPA cells IFN-γ-dependent STAT1 signaling may play a central role in shaping the tumor microenvironment, with A20 loss enhancing expression of downstream targets. To assess whether this phenotype extends to other EGFR-driven LUAD cell lines we analyzed STAT1 expression and STAT1-avtivating Y701 phosphorylation (pSTAT1) in H1975-WT and H1975-ΔA20 cells prior to and after 15 min of stimulation with IFN-γ (10 ng/mL) (Fig. 15A). Western blot analysis of STAT1 expression in H1975-WT cells revealed no detectable expression of STAT1, with and without IFN-γ stimulation. In H1975-ΔA20 cells STAT1 expression was detected in both stimulated and unstimulated cells. Furthermore pSTAT1(Y701) was not detected in H1975-WT cells, whereas a faint band was observed in H1975-ΔA20 prior to stimulation and a strong band was visible after stimulation, indicating loss of A20 also enhances STAT1 activation in this cell line. Furthermore, we inspected expression and activation of STAT3, as tumor-intrinsic STAT3 signaling is often associated with tumor survival and proliferation.[106] In both H1975-WT and ΔA20 cells STAT3 levels were comparable, even after IFN-γ stimulation (Fig. 15B). In H1975-WT cells however, pSTAT3(Y705) levels seemed to be lower compared to H1975-ΔA20. IFN-γ stimulation did not have a significant effect on STAT3 phosphorylation. To assess whether the lower expression of STAT1 is confined to a protein level or also detectable on a mRNA level RT-qPCR was performed. Indeed, *STAT1*-mRNA was upregulated in H1975-ΔA20 compared to WT cells (Fig. 15C). Furthermore, we assessed mRNA-expression of *CD274* (encoding PD-L1). *CD274* expression was downregulated in ΔA20 cells, compared to WT cells (Fig. 15D). Given a substantial change gene expression pattern, particularly in STAT1-dependent signaling we aimed to determine if loss of A20 changes the proliferative behavior of H1975 cells. A proliferation assay, visualized by crystal violet staining revealed a lower proliferation rate of H1975-ΔA20 cells, compared to their wild-type counterparts (Fig. 15E). Since H1975 cells harbor the activating EGFR mutations L858R and T790M, we sought to investigate whether loss of A20 could affects sensitivity to EGFR inhibition. We treated H1975-WT and ΔA20 cells with osimertinib and determined the half-maximal inhibitory concentration (IC_{50}).

We determined an IC_{50} of 8.399 nM for H1975-WT cells and an IC_{50} of 40.67 nM for H1975-ΔA20 (Fig. 15F). This suggests that the loss of A20 reduces sensitivity to osimertinib by approximately five-fold, indicating a potential role of A20 in modulating drug responsiveness.

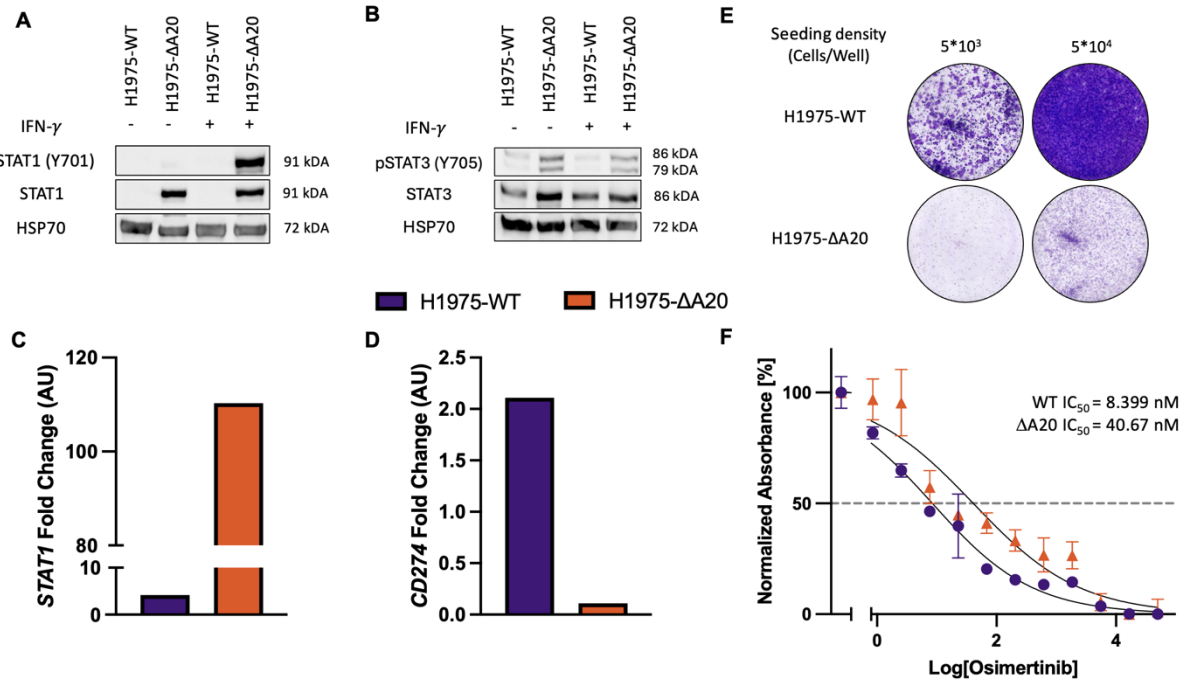

Figure 15: (A) Western Blot of pSTAT1(Y701) and STAT1 in H1975-WT and H1975-ΔA20 cells prior and post IFN-γ stimulation (15 min, 10 ng/mL). HSP70 was used as a housekeeping control. **(B)** Western Blot of pSTAT3(Y705) and STAT3 in H1975-WT and H1975-ΔA20 cells prior and post IFN-γ stimulation (15 min, 10 ng/mL). HSP70 was used as a housekeeping control. **(C)** Fold change in STAT1 expression, **(D)** fold change in CD276 expression fold change in H1975-WT and H1975-ΔA20 cells after 8 hours of IFN-γ stimulation (10 ng/mL), compared to unstimulated controls, assessed by RT-qPCR. **(E)** Crystal violet staining following a 3-day proliferation assay of H1975-WT and H1975-ΔA20 cells seeded at two different densities (5×10³ and 5×10⁴ cells per well). **(F)** MTT cell viability assay and determination of IC50 of H1975-WT and H1975-ΔA20 cells with osimertinib treatment (3 days).

Discussion

The role of A20 in LUAD is dependent on the driver-mutation

A20 seems to have a dual role in lung adenocarcinoma. In contrast to KRAS-mutant LUAD, where a potent tumor suppressive effect of A20 was previously demonstrated,[86] A20 seems to have an oncogenic role in EGFR-mutant LUAD. In immunogenic, OVA-expressing EGFR-mutant tumors, loss of A20 leads to a significantly reduced tumor burden and increased survival *in vivo*. The inclusion of OVA in this model ensures immune recognition of the tumors, as without OVA no difference in tumor burden could be detected upon A20 knockout.

The inclusion of OVA as a tumor neoantigen itself does not account for the oncogenic function of A20 in EGFR-mutant LUAD, as demonstrated by the inclusion of OVA in the KRAS-driven tumor model. In this context OVA did not alter the tumor suppressive effect of A20, which was previously described in *Breitenecker et al*., suggesting that the oncogenic role of A20 in EGFR-driven LUAD is context-dependent and not merely a result of OVA-mediated, enhanced immunogenicity.[86]

Interestingly, despite the opposing phenotypes observed in KRAS- and EGFR-driven LUAD upon loss of A20 transcriptomic analysis revealed no major variance in differentially expressed pathways. This suggests that A20's role is not determined by large-scale transcriptional differences between KRAS- and EGFR tumors. This is in accordance with the fact that mutations in KRAS and EGFR lead to the activation of similar downstream pathways, mainly the Mitogen-Activated Protein Kinase (MAPK) and PI3K pathways, which may explain the similar gene expression profiles upon loss of A20.

Loss of A20 affects later tumor progression rather than initiation

The tumor area 11 weeks after tumor initiation was relatively low, ranging between 0% and 5.5%. No statistical differences in tumor number and tumor area could be detected between the groups, although some mice with EPOA tumors tended to have a slightly higher tumor burden than the other groups. The absence of a significant difference in tumor burden after 11 weeks suggests that A20 does not impact tumorigenesis and initial tumor growth. Only seven weeks later however, a significant reduction of tumor burden in mice with EPOA tumor was observed, suggesting A20 may play a more prominent role in later stages of tumor progression. One way in which the lack of A20 may stunt tumor growth is by altering the tumor immune infiltrate. Flow cytometry analysis of whole lungs showed a slight decrease of $CD3^+$ T cells in lungs with EPOA tumors 11 weeks after tumor initiation and an increase in total $F4/80^+$ macrophages in EPOA tumors. Furthermore, lungs bearing EPOA tumors showed a slight decrease in $CD206^+$ macrophage abundance. Additionally, IHC analysis showed a lower number of $CD8^+$ cytotoxic T cells within EPOA tumors, when compared to EPO tumors. These observations are in accordance with the trend of slightly higher tumor burden in mice with EPOA tumors after 11 weeks. A decrease of T cells in the lung environment and specifically a lower number of $CD8^+$ T cells may contribute to an initial faster tumor progression in the early stages of tumor growth. These trends, however, are reversed by 18 weeks after tumor initiation. IHC analysis shows a clear increase in $CD4^+$ and $CD8^+$ T cells and a decrease of $F4/80^+$ and $CD206^+$ macrophages in EPOA tumors, compared to EPO tumors. This shift in the composition of the TME between 11 and 18 weeks may be a key factor in contributing to the significantly lower tumor burden in EPOA mice. Especially the higher number of T cells in EPOA tumors suggests increased immune recognition of these tumors. High A20 expression was previously linked to a tumor suppressive immune phenotype, with increased $CD8^+$ T cell, macrophage and NK cell abundance in KRAS-mutant LUAD, resulting in reduced tumor burden.[86] In contrast, in EGFR-driven tumors we observe a higher tumor burden associated with A20 expression and our TME analysis supports a pro-tumorigenic role in the EGFR-context. Given the dual role of A20 in various types of cancer other studies have linked A20 expression with a poor immune cell infiltration and impaired antitumor response, for example in colorectal cancer[107] and melanoma.[108]

T Cells Mediate the Anti-Tumor Effect of A20 Deficiency

Our findings in Rag2$^{-/-}$ mice highlight the importance of T cells in mediating the anti-tumor immune response in A20-deficient EGFR-driven tumors. Tumor growth was significantly different after intratracheal transplantation of EP and EPA cells. Mice with EPA tumors showed a significantly higher tumor burden than EP mice. In the absence of T cells, the loss of A20 leads to the opposite phenotype compared to what was observed in immunocompetent mice. This difference in tumor growth is likely not due to a cell-intrinsic effect of A20 loss but rather reflects the absence of T cell-mediated immune control in the Rag2^{-}/$^{-}$ setting, as evidenced by data generated by *Seungyeon Lim*.[109] In an *in vitro* proliferation assay, EPA cells showed a significantly slower proliferation than EP cells. Additionally, these cells were transplanted subcutaneously in immunodeficient NOD scid gamma (NSG) mice. In this setting and in the autochthonous tumor model in C57BL/6N mice EPA tumors also showed reduced tumor growth. These results may suggest that in the Rag2^{-}/$^{-}$ context the remaining immune cell populations such as macrophages or other myeloid cells may boost tumor growth of A20-deficient tumor cells. Lymphocytes like T cells may counteract this effect when present, however further research is needed to address this question.

A20 alters expression of genes involved in T cell function

A possible explanation for increased immunogenicity upon loss of A20 is an enhanced sensitivity of tumor cells to IFN-γ signaling, leading to the expression of immunologically relevant genes. Western blot analysis of EP and EPA cells showed increased STAT1 expression in EPA cells (data generated by *Seungyeon Lim*),[109] a key regulator in anti-tumorigenic immune responses.[110] Expression analysis by RNA-seq revealed differences in expression of several genes involved in T cell recruitment and activation in EPA cells, compared to EP cells. Even though expression of *Stat1* or *Stat3* was not significantly altered, Jak2 expression was increased in EPA cells. This indicates that loss of A20 may not directly enhance STAT1 or STAT3 protein levels but rather contribute to increased signaling by enhancing STAT1 or STAT3 phosphorylation via JAK2. EPA cells showed a significant increase in expression of *Cxcl10* and *Il15*. CXCL10 is a ligand that binds to CXCR3, a chemokine receptor, for which a role in CD8^{+} T cell trafficking to tumors has been directly demonstrated.[111]

Studies have shown that increased NF-κB signaling, significantly promotes CXCL10 expression.[112,113] This was also demonstrated in a human LUAD cell line.[114] Loss of A20 in EPA cells could therefore lead to higher CXCL10 expression via increased NF-κB signaling. IL-15, on the other hand, is a cytokine which was shown to enhance the antitumor activity of tumor-reactive cytotoxic $CD8^+$ T cells.[103] Elevated expression of *Cxcl10* and *Il15* may be key contributors in the elevated T cell-mediated immunity in A20-deficient EGFR tumors. Expression of *Tap1* and *Tap2* were not significantly altered in EPA cells compared to EP cells. MHC-1 levels on the cell surface, determined by flow cytometry were slightly increased in EPA cells, suggesting that loss of A20 only has limited effects on MHC-1 antigen presentation. The increased levels of Icam1 and Vcam1 in EPA cells may further contribute to the enhanced T cell infiltration observed in A20-deficient tumors. Adhesion molecules like ICAM-1 and VCAM-1 however can have different effects on tumor immunogenicity or tumor progression. ICAM-1 for example can on the one hand promote immune evasion and metastasis, but on the other hand drive immune cell migration, infiltration and forming immunological synapses.[115] VCAM-1 has a more complex role in cancer, as its expression was also shown to correlate with T cell infiltration in certain tumor models,[116] however it is also associated with tumor progression and immune evasion.[117] In human patients, high expression of ICAM-1 and VCAM-1 has been shown to correlate to higher $CD8^+$ T cell levels and prolonged survival in colorectal cancer.[118] While enhanced expression of adhesion molecules alone may not be sufficient to drive T cell infiltration, it can act synergistically with chemokines and antigen presentation. In a study on melanoma high expression of CXCL10 was associated with ICAM-1 and VCAM-1 expression, which promoted T cell migration.[119] While *Cd274* (PD-L1) mRNA expression was not significantly altered upon loss of A20 in the RNA-seq data, a slight increase in cell surface PD-L1 expression could be observed by flow cytometry in EPA cells. However, expression of another immune checkpoint inhibitor, *Cd276*, was significantly downregulated in EPA cells, compared to EP cells. Overexpression of CD276 is observed in many cancers and promotes immune evasion by exclusion of T cells from the TME.[120] Most of the differentially expressed genes observed in the RNA-seq data support the notion that loss of A20 leads to an altered expression of genes involved in T cell recruitment and activation and therefore increased T cell-mediated anti-tumor immunity.

Having established that loss of A20 leads to enhanced T cell infiltration in EGFR-driven tumors, we aimed to understand the opposite phenotype observed in KRAS-driven tumors, where loss of A20 resulted in reduced T cell infiltration. GSEA did not reveal major differences in global immune-related pathway up- or downregulation between EPA and KPA cells, suggesting that the phenotypic difference may be mediated by differential regulation of a few key genes. Indeed, we observed striking differences in expression of *Stat1*, *Stat3* and *Jak2*. While *Stat1* and *Stat3* were upregulated in EPA cells, *Jak2* was downregulated in EPA cells. Among these, *Stat1* may play a significant role in promoting immune cell infiltration, given its role as a key regulator of cytokine expression and promotion of antigen presentation. Furthermore, expression of *Cxcl10* was significantly higher in EPA cells compared to KPA cells. This downregulation of *Cxcl10* in KRAS-mutated cancers was previously observed in colorectal cancer[121] and in lung cancer, where Histone Deacetylase 3 (HDAC3) restricts expression of *Cxcl10* and other genes, associated with T cell recruitment.[122] The slightly increased *Tap1* expression in EPA cells may contribute to enhanced antigen presentation. *Vcam1* expression was significantly elevated in KPA cells, however since pro- and antitumorigenic effects of VCAM-1 expression in cancer have been reported[123], its role in in modulating immune cell infiltration in this model remains unclear. PD-L1 expression (*Cd274*) was elevated in KPA cells, consistent with previously findings showing increased PD-L1 expression in KRAS-mutated lung tumor cells upon loss of A20.[86] Interestingly, *Cd276* levels however were significantly increased in EPA cells compared to KPA cells, which seems inconsistent with the higher T cell infiltration observed in EGFR-tumors. Increased expression of this immune checkpoint molecule may be a response to sustained T cell infiltration, as IFN-γ, produced by T cells initiates *Cd276* expression in tumor cells.[124]

Together these findings suggest that the opposing phenotypes observed upon A20 loss in EGFR- and KRAS-driven tumors may be driven by differential expression of a limited number of immune-regulatory genes, rather than global changes in gene expression.

Functional impact of A20 deficiency in human EGFR-LUAD cells

As observed in murine EGFR-mutant cells (EPA), STAT1 phosphorylation is significantly upregulated in human H1975 cells upon loss of A20 and IFN-γ stimulation. This finding was confirmed by Western blot and RT-qPCR. STAT1 target gene CD274*,* however showed a lower mRNA expression in H1975-ΔA20 cells, compared to H1975-WT cells. The downregulation of CD274*,* may promote a TME more favorable for immune cell infiltration. This hypothesis, however, would need to be further tested, for example by intratracheal transplantation of H1975-WT and H1975-ΔA20 *in vivo* and IHC analysis. The mechanism by which expression of CD274 is downregulated, despite increased STAT1 activation is unclear, however other pathways such as RAS-RAF-MEK or PI3K, also play a significant role in controlling CD274.[125] Not only was STAT1 phosphorylation shown to be upregulated in H1975-ΔA20, but also STAT3 phosphorylation, although to a lesser extent. STAT3 activation in cancer cells often induces expression of genes promoting cellular proliferation, immune evasion and resistance against apoptosis or angiogenesis. STAT3 activation seems to be higher in H1975-ΔA20 cells. This may be a counter mechanism to the increased STAT1 activation, which usually is associated with anti-tumorigenic immunity.[126] Furthermore, a proliferation assay showed a stark difference in proliferative activity between H1975-WT and H1975-ΔA20 cells. In a crystal violet assay, we observed a slower growth rate of H1975-ΔA20 cells, suggesting that A20 expression may support tumor cell proliferation. By determining the IC_{50} of WT and ΔA20 cells in response to osimertinib we quantified an approximately 5-fold decrease in sensitivity upon loss of A20. This finding suggests that A20 expression levels may be associated with altered sensitivity to osimertinib. However, further studies are required to determine whether A20 may represent a predictive biomarker for osimertinib response.

Clinical implications

Our findings support an oncogenic role of A20 in EGFR-driven LUAD, by modulating the TME to favor immune evasion and tumor progression, specifically by limiting T cell infiltration and recognition of the tumors. However, the mechanism by which A20 facilitates this phenotype remains unclear. Based on available patient data, it was observed that A20 is frequently downregulated in human EGFR-cancers. The expression level of A20 may represent a potential prognostic biomarker in the future, as lower A20 expression and therefore increased tumor infiltration by $CD8^+$ T cells may enhance ICB outcomes. Supporting this hypothesis, a study conducted on colorectal cancer has shown that downregulation of A20 led to an improved antitumor response and higher efficacy of α-PD-L1 therapy.[107] Another study, conducted on melanoma found similar results, but additionally showed that targeting A20 with siRNAs in A20-expressing tumors improves the antitumor capacity of $CD8^+$ T cells and promoted α-PD-L1 therapy response[108]. These findings suggest that targeting A20 could improve the efficacy of immune checkpoint blockade therapy outcomes in patients in the future. Targeting A20 with traditional small molecule inhibitors, however, may not be a viable option, as A20 has multiple functional domains. One potential future approach may be targeting A20 with proteolysis-targeting chimeras (PROTACs), molecules which recruit E3 ubiquitin ligases to specific proteins to tag them for proteasomal degradation. As of 2025 no PROTAC has been clinically approved, but several PROTACs are undergoing clinical trials for cancer treatment.[127] A further option for targeting A20 are small-interfering RNAs (siRNAs). siRNAs are designed to specifically bind a target-mRNA, leading to its degradation and thereby inhibiting protein translation. As with PROTACs, no siRNA-based therapy has been clinically approved so far, but several are in ongoing clinical trials.[128] These technologies may be implemented to target A20 in the future, however, further *in vivo* studies are necessary to determine how A20-deficient and A20-proficient tumors respond to ICB therapy in EGFR-driven LUAD.

Limitations of the study

While this thesis provides new insights into the role of A20 in EGFR-driven LUAD there are several limitations, that need to be addressed. We primarily focused on analyzing the role of T cells, even though a significant decrease in macrophage infiltration upon A20 loss was observed in our IHC analysis. Macrophages and other cell types, like NK cells or dendritic cells, may also contribute significantly to the observed phenotype.

Because IHC analysis results between the 11-week and 18-week timepoint differ greatly, analysis of another timepoint (e.g. 15 weeks) would be necessary to accurately characterize the dynamics of the changes within the TME over time.

Although RNA-seq analysis revealed differential gene expression of some genes related to T cell function or recruitment, these findings likely provide only a limited explanation of the role of A20 in modulating the immune infiltrate within tumors. While the analyzed factors may contribute to T cell infiltration, they are probably not the only ones responsible, as immune cell infiltration in tumors is regulated by a more complex interplay between tumor cells, stroma cells and various immune cells. Furthermore, the expression of these genes was only examined on a mRNA level. Additional expression analysis on a protein level could validate whether the observed changes in mRNA transcription translate to functional differences.

One aspect important to note is the use of an autochthonous mouse model. While it closely replicates the natural process of tumor initiation by induction of mutations in lung epithelial cells and allows us to study tumor progression and tumor-immune system interactions in its native environment, it also has limitations. Mouse models like the one used in this study have a low mutational burden and often lack strong neoantigens and thereby fails to accurately mimic the complexity of human lung tumors, which typically have a high mutational burden.[95] To counteract the lack of neoantigens in this model the expression of OVA was included to ensure immune recognition of the tumors, however it remains unclear whether OVA expression is maintained throughout the course of the experiment, as downregulation would pose a significant advantage by avoiding immune recognition.

References

1. Bray Bsc F, Laversanne | Mathieu, Hyuna |, et al. Global cancer statistics 2022: GLOBOCAN estimates of incidence and mortality worldwide for 36 cancers in 185 countries. *CA Cancer J Clin*. 2024;74(3):229-263. doi:10.3322/CAAC.21834

2. Zheng R, Wang S, Zhang S, et al. Global, regional, and national lifetime probabilities of developing cancer in 2020. *Sci Bull (Beijing)*. 2023;68(21):2620. doi:10.1016/J.SCIB.2023.09.041

3. Bizuayehu HM, Ahmed KY, Kibret GD, et al. Global Disparities of Cancer and Its Projected Burden in 2050. *JAMA Netw Open*. 2024;7(11):e2443198. doi:10.1001/JAMANETWORKOPEN.2024.43198

4. Sung H, Ferlay J, Siegel RL, et al. Global Cancer Statistics 2020: GLOBOCAN Estimates of Incidence and Mortality Worldwide for 36 Cancers in 185 Countries. *CA Cancer J Clin*. 2021;71(3):209-249. doi:10.3322/CAAC.21660

5. Estape T. Cancer in the Elderly: Challenges and Barriers. *Asia Pac J Oncol Nurs*. 2018;5(1):40. doi:10.4103/APJON.APJON_52_17

6. Boffetta P, Nyberg F. Contribution of environmental factors to cancer risk. *Br Med Bull*. 2003;68(1):71-94. doi:10.1093/BMP/LDG023

7. Board I of M (US) and NRC (US) NCP, Curry SJ, Byers T, Hewitt M. Lifestyle Behaviors Contributing to the Burden of Cancer. In: National Academies Press (US); 2003. Accessed March 24, 2025. https://www.ncbi.nlm.nih.gov/books/NBK223925/

8. Warren GW, Cummings KM. Tobacco and lung cancer: risks, trends, and outcomes in patients with cancer. *Am Soc Clin Oncol Educ Book*. 2013;(33):359-364. doi:10.14694/EDBOOK_AM.2013.33.359

9. Tzu-Hsuan Chen D, Hirst J, C Coupland CA, Liao W, Baldwin DR, Hippisley-Cox J. Ethnic disparities in lung cancer incidence and differences in diagnostic characteristics: a population-based cohort study in England. *The Lancet Regional Health - Europe*. Published online 2025. doi:10.1016/j.lanepe.2024.101124

10. Kanwal M, Ding XJ, Cao Y. Familial risk for lung cancer. *Oncol Lett*. 2016;13(2):535. doi:10.3892/OL.2016.5518

11. Hecht SS. Lung carcinogenesis by tobacco smoke. *Int J Cancer*. 2012;131(12):2724-2732. doi:10.1002/IJC.27816

12. Jha P. Avoidable global cancer deaths and total deaths from smoking. *Nature Reviews Cancer 2009 9:9*. 2009;9(9):655-664. doi:10.1038/nrc2703

13. Lee JM, Yanagawa J, Peebles KA, Sharma S, Mao JT, Dubinett SM. Inflammation in lung carcinogenesis: New targets for lung cancer chemoprevention and treatment. *Crit Rev Oncol Hematol*. 2008;66(3):208-217. doi:10.1016/J.CRITREVONC.2008.01.004

14. Greenman C, Stephens P, Smith R, et al. Patterns of somatic mutation in human cancer genomes. *Nature 2006 446:7132*. 2007;446(7132):153-158. doi:10.1038/nature05610

15. Keith RJ, Fetterman JL, Orimoloye OA, et al. Characterization of Volatile Organic Compound Metabolites in Cigarette Smokers, Electronic Nicotine Device Users, Dual Users, and Nonusers of Tobacco. *Nicotine & Tobacco Research*. 2019;22(2):264. doi:10.1093/NTR/NTZ021

16. Shankar A, Dubey A, Saini D, et al. Environmental and occupational determinants of lung cancer. *Transl Lung Cancer Res*. 2019;8(Suppl 1):S31. doi:10.21037/TLCR.2019.03.05

17. Wang Q. Urbanization and Global Health: The Role of Air Pollution. *Iran J Public Health*. 2018;47(11):1644. Accessed May 20, 2025. https://pmc.ncbi.nlm.nih.gov/articles/PMC6294869/

18. Xue Y, Wang L, Zhang Y, Zhao Y, Liu Y. Air pollution: A culprit of lung cancer. *J Hazard Mater*. 2022;434:128937. doi:10.1016/J.JHAZMAT.2022.128937

19. de Alencar VTL, Figueiredo AB, Corassa M, Gollob KJ, Cordeiro de Lima VC. Lung cancer in never smokers: Tumor immunology and challenges for immunotherapy. *Front Immunol*. 2022;13:984349. doi:10.3389/FIMMU.2022.984349

20. You M, Wang D, Liu P, et al. Fine mapping of chromosome 6q23-25 region in familial lung cancer families reveals RGS17 as a likely candidate gene. *Clinical Cancer Research*. 2009;15(8):2666-2674. doi:10.1158/1078-0432.CCR-08-2335

21. Wang J, Liu Q, Yuan S, et al. Genetic predisposition to lung cancer: comprehensive literature integration, meta-analysis, and multiple evidence assessment of candidate-gene association studies. *Scientific Reports 2017 7:1*. 2017;7(1):1-13. doi:10.1038/s41598-017-07737-0

22. Vogelstein B, Papadopoulos N, Velculescu VE, Zhou S, Diaz LA, Kinzler KW. Cancer genome landscapes. *Science*. 2013;339(6127):1546-1558. doi:10.1126/SCIENCE.1235122

23. Xia L, Wang Z, Wu X, et al. Multiplatform discovery and regulatory function analysis of structural variations in non-small cell lung carcinoma. *Cell Rep*. 2021;36(10):109660. doi:10.1016/J.CELREP.2021.109660

24. Ahrendt SA, Decker PA, Doffek K, et al. Microsatellite instability at selected tetranucleotide repeats is associated with p53 mutations in non-small cell lung cancer. *Cancer Res*. 2000;60(9):2488-2491.

25. Minna JD. The molecular biology of lung cancer pathogenesis. *Chest*. 1993;103(4 SUPPL.):449S-456S. doi:10.1378/chest.103.4_Supplement.449S

26. Riihimäki M, Hemminki A, Fallah M, et al. Metastatic sites and survival in lung cancer. *Lung Cancer*. 2014;86(1):78-84. doi:10.1016/J.LUNGCAN.2014.07.020

27. Popper HH. Progression and metastasis of lung cancer. *Cancer and Metastasis Reviews 2016 35:1*. 2016;35(1):75-91. doi:10.1007/S10555-016-9618-0

28. Zheng M. Classification and Pathology of Lung Cancer. *Surg Oncol Clin N Am*. 2016;25(3):447-468. doi:10.1016/J.SOC.2016.02.003

29. Sánchez-Ortega M, Carrera AC, Garrido A. Role of NRF2 in Lung Cancer. *Cells 2021, Vol 10, Page 1879*. 2021;10(8):1879. doi:10.3390/CELLS10081879

30. Hynds RE, Frese KK, Pearce DR, Grönroos E, Dive C, Swanton C. Progress towards non-small-cell lung cancer models that represent clinical evolutionary trajectories: NSCLC pre-clinical models. *Open Biol*. 2021;11(1). doi:10.1098/RSOB.200247/

31. Travis WD, Brambilla E, Nicholson AG, et al. The 2015 World Health Organization Classification of Lung Tumors: Impact of Genetic, Clinical and Radiologic Advances since the 2004 Classification. *Journal of Thoracic Oncology*. 2015;10(9):1243-1260. doi:10.1097/JTO.0000000000000630

32. Hutchinson BD, Shroff GS, Truong MT, Ko JP. Spectrum of Lung Adenocarcinoma. *Seminars in Ultrasound, CT and MRI*. 2019;40(3):255-264. doi:10.1053/J.SULT.2018.11.009

33. Devarakonda S, Li Y, Rodrigues FM, et al. Genomic Profiling of Lung Adenocarcinoma in Never-Smokers. *Journal of Clinical Oncology*. 2021;39(33):3747-3758. doi:10.1200/JCO.21.01691

34. Weir BA, Woo MS, Getz G, et al. Characterizing the cancer genome in lung adenocarcinoma. *Nature 2007 450:7171*. 2007;450(7171):893-898. doi:10.1038/nature06358

35. Brzeziańska E, Dutkowska A, Antczak A. The significance of epigenetic alterations in lung carcinogenesis. *Molecular Biology Reports 2012 40:1*. 2012;40(1):309-325. doi:10.1007/S11033-012-2063-4

36. Suster DI, Mino-Kenudson M. Molecular Pathology of Primary Non-small Cell Lung Cancer. *Arch Med Res*. 2020;51(8):784-798. doi:10.1016/J.ARCMED.2020.08.004

37. Skoulidis F, Heymach J V. Co-occurring genomic alterations in non-small-cell lung cancer biology and therapy. *Nature Reviews Cancer 2019 19:9*. 2019;19(9):495-509. doi:10.1038/s41568-019-0179-8

38. Devarakonda S, Morgensztern D, Govindan R. Genomic alterations in lung adenocarcinoma. *Lancet Oncol*. 2015;16(7):e342-e351. doi:10.1016/S1470-2045(15)00077-7.

39. Riely GJ, Kris MG, Rosenbaum D, et al. Frequency and Distinctive Spectrum of KRAS Mutations in Never Smokers with Lung Adenocarcinoma. *Clin Cancer Res*. 2008;14(18):5731. doi:10.1158/1078-0432.CCR-08-0646

40. Singh B, Carpenter G, Coffey RJ. EGF receptor ligands: recent advances. *F1000Research 2016 5:2270*. 2016;5:2270. doi:10.12688/f1000research.9025.1

41. Da Cunha Santos G, Shepherd FA, Tsao MS. EGFR mutations and lung cancer. *Annual Review of Pathology: Mechanisms of Disease*. 2011;6(Volume 6, 2011):49-69. doi:10.1146/ANNUREV-PATHOL-011110-130206

42. Wells A. EGF receptor. *Int J Biochem Cell Biol*. 1999;31(6):637-643. doi:10.1016/S1357-2725(99)00015-1

43. Quinlan M, Settleman J. Isoform-Specific Ras Functions in Development and Cancer. *Future Oncology*. 2009;5(1):105-116. doi:10.2217/14796694.5.1.105

44. Prior IA, Lewis PD, Mattos C. A comprehensive survey of Ras mutations in cancer. *Cancer Res*. 2012;72(10):2457. doi:10.1158/0008-5472.CAN-11-2612

45. Uniyal P, Kashyap VK, Behl T, Parashar D, Rawat R. KRAS Mutations in Cancer: Understanding Signaling Pathways to Immune Regulation and the Potential of Immunotherapy. *Cancers 2025, Vol 17, Page 785*. 2025;17(5):785. doi:10.3390/CANCERS17050785

46. Harrison PT, Vyse S, Huang PH. Rare epidermal growth factor receptor (EGFR) mutations in non-small cell lung cancer. *Semin Cancer Biol*. 2020;61:167. doi:10.1016/J.SEMCANCER.2019.09.015

47. Zhang Z, Stiegler AL, Boggon TJ, Kobayashi S, Halmos B. EGFR-mutated lung cancer: a paradigm of molecular oncology. *Oncotarget*. 2010;1(7):497. doi:10.18632/ONCOTARGET.186

48. Westcott PMK, To MD. The genetics and biology of KRAS in lung cancer. *Chin J Cancer*. 2013;32(2):63. doi:10.5732/CJC.012.10098

49. Karachaliou N, Mayo C, Costa C, et al. KRAS Mutations in Lung Cancer. *Clin Lung Cancer*. 2013;14(3):205-214. doi:10.1016/J.CLLC.2012.09.007

50. Huang L, Guo Z, Wang F, Fu L. KRAS mutation: from undruggable to druggable in cancer. *Signal Transduction and Targeted Therapy 2021 6:1*. 2021;6(1):1-20. doi:10.1038/s41392-021-00780-4

51. Ash LJ, Busia-Bourdain O, Okpattah D, Kamel A, Liberchuk A, Wolfe AL. KRAS: Biology, Inhibition, and Mechanisms of Inhibitor Resistance. *Current Oncology 2024, Vol 31, Pages 2024-2046*. 2024;31(4):2024-2046. doi:10.3390/CURRONCOL31040150

52. Sung WJ, Kim D, Zhu A, et al. The lysosome as a novel therapeutic target of EGFR-mediated tumor inflammation. *Front Pharmacol*. 2022;13. doi:10.3389/FPHAR.2022.1050758

53. Tran PN, Klempner SJ. Profile of rociletinib and its potential in the treatment of non-small-cell lung cancer. *Lung Cancer: Targets and Therapy*. 2016;7:91. doi:10.2147/LCTT.S94337

54. Karachaliou N, Fernandez-Bruno M, Bracht JWP, Rosell R. EGFR first- and second-generation TKIs—there is still place for them in EGFR-mutant NSCLC patients. *Transl Cancer Res*. 2019;8(Suppl 1):S23. doi:10.21037/TCR.2018.10.06

55. Tan CS, Kumarakulasinghe NB, Huang YQ, et al. Third generation EGFR TKIs: Current data and future directions. *Mol Cancer*. 2018;17(1):1-14. doi:10.1186/S12943-018-0778-0

56. Gomatou G, Syrigos N, Kotteas E. Osimertinib Resistance: Molecular Mechanisms and Emerging Treatment Options. *Cancers 2023, Vol 15, Page 841*. 2023;15(3):841. doi:10.3390/CANCERS15030841

57. Chhouri H, Alexandre D, Grumolato L. Mechanisms of Acquired Resistance and Tolerance to EGFR Targeted Therapy in Non-Small Cell Lung Cancer. *Cancers (Basel)*. 2023;15(2):504. doi:10.3390/CANCERS15020504

58. Cheng Z, Cui H, Wang Y, et al. The advance of the third-generation EGFR-TKI in the treatment of non-small cell lung cancer. *Oncol Rep*. 2024;51(1):1-13. doi:10.3892/OR.2023.8675

59. Takeda M, Nakagawa K. First- and Second-Generation EGFR-TKIs Are All Replaced to Osimertinib in Chemo-Naive EGFR Mutation-Positive Non-Small Cell Lung Cancer? *Int J Mol Sci*. 2019;20(1):146. doi:10.3390/IJMS20010146

60. Corvaja C, Passaro A, Attili I, et al. Advancements in fourth-generation EGFR TKIs in EGFR-mutant NSCLC: Bridging biological insights and therapeutic development. *Cancer Treat Rev*. 2024;130:102824. doi:10.1016/J.CTRV.2024.102824

61. Wieder T, Eigentler T, Brenner E, Röcken M. Immune checkpoint blockade therapy. *Journal of Allergy and Clinical Immunology*. 2018;142(5):1403-1414. doi:10.1016/J.JACI.2018.02.042

62. Li Y, Hu L, Peng X, Xu H, Tang B, Xu C. Resistance to immune checkpoint inhibitors in KRAS-mutant non-small cell lung cancer. *Cancer Drug Resistance*. 2022;5(1):129. doi:10.20517/CDR.2021.102

63. Uras IZ, Moll HP, Casanova E. Targeting KRAS Mutant Non-Small-Cell Lung Cancer: Past, Present and Future. *International Journal of Molecular Sciences 2020, Vol 21, Page 4325*. 2020;21(12):4325. doi:10.3390/IJMS21124325

64. Cox AD, Der CJ. “Undruggable KRAS”: druggable after all. *Genes Dev*. 2024;39(1-2):132-162. doi:10.1101/GAD.352081.124

65. Ostrem JM, Peters U, Sos ML, Wells JA, Shokat KM. K-Ras(G12C) inhibitors allosterically control GTP affinity and effector interactions. *Nature 2013 503:7477*. 2013;503(7477):548-551. doi:10.1038/nature12796

66. Arnson Y, Shoenfeld Y, Amital H. Effects of tobacco smoke on immunity, inflammation and autoimmunity. *J Autoimmun*. 2010;34(3):J258-J265. doi:10.1016/J.JAUT.2009.12.003

67. Azad N, Rojanasakul Y, Vallyathan V. Inflammation and Lung Cancer: Roles of Reactive Oxygen/Nitrogen Species. *Journal of Toxicology and Environmental Health, Part B*. 2008;11(1):1-15. doi:10.1080/10937400701436460

68. Demir AB. Tumor Promoting Inflammation. *Current Molecular Biology Reports 2023 9:3*. 2023;9(3):21-32. doi:10.1007/S40610-023-00153-6

69. Jayasingam SD, Citartan M, Thang TH, Mat Zin AA, Ang KC, Ch’ng ES. Evaluating the Polarization of Tumor-Associated Macrophages Into M1 and M2 Phenotypes in Human Cancer Tissue: Technicalities and Challenges in Routine Clinical Practice. *Front Oncol*. 2020;9:494426. doi:10.3389/FONC.2019.01512

70. Altorki NK, Markowitz GJ, Gao D, et al. The lung microenvironment: an important regulator of tumour growth and metastasis. *Nature Reviews Cancer 2018 19:1*. 2018;19(1):9-31. doi:10.1038/s41568-018-0081-9

71. Schulze AB, Evers G, Görlich D, et al. Tumor infiltrating T cells influence prognosis in stage I–III non-small cell lung cancer. *J Thorac Dis*. 2020;12(5):1824. doi:10.21037/JTD-19-3414A

72. McKenzie B, Valitutti S. Resisting T cell attack: tumor-cell-intrinsic defense and reparation mechanisms. *Trends Cancer*. 2023;9(3):198-211. doi:10.1016/J.TRECAN.2022.12.003

73. Catrysse L, Vereecke L, Beyaert R, van Loo G. A20 in inflammation and autoimmunity. *Trends Immunol*. 2014;35(1):22-31. doi:10.1016/J.IT.2013.10.005

74. Verstrepen L, Verhelst K, van Loo G, Carpentier I, Ley SC, Beyaert R. Expression, biological activities and mechanisms of action of A20 (TNFAIP3). *Biochem Pharmacol*. 2010;80(12):2009-2020. doi:10.1016/J.BCP.2010.06.044

75. Shi Y, Wang X, Wang J, Wang X, Zhou H, Zhang L. The dual roles of A20 in cancer. *Cancer Lett*. 2021;511:26-35. doi:10.1016/J.CANLET.2021.04.017

76. Wertz IE, O'Rourke KM, Zhou H, et al. De-ubiquitination and ubiquitin ligase domains of A20 downregulate NF-κB signalling. *Nature 2004 430:7000*. 2004;430(7000):694-699. doi:10.1038/nature02794

77. Skaug B, Chen J, Du F, He J, Ma A, Chen ZJ. Direct, Non-catalytic Mechanism of IKK Inhibition by A20. *Mol Cell*. 2011;44(4):559. doi:10.1016/J.MOLCEL.2011.09.015

78. Moll HP, Lee A, Minussi DC, et al. A20 Regulates Atherogenic Interferon (IFN)-γ Signaling in Vascular Cells by Modulating Basal IFNβ Levels. *Journal of Biological Chemistry*. 2014;289(45):30912-30924. doi:10.1074/JBC.M114.591966

79. Bhattacharyya S, Wang W, Graham LVD, Varga J. A20 suppresses canonical Smad-dependent fibroblast activation: novel function for an endogenous inflammatory modulator. *Arthritis Res Ther*. 2016;18(1). doi:10.1186/S13075-016-1118-7

80. Priem D, van Loo G, Bertrand MJM. A20 and Cell Death-driven Inflammation. *Trends Immunol*. 2020;41(5):421-435. doi:10.1016/J.IT.2020.03.001

81. Ma A, Malynn BA. A20: linking a complex regulator of ubiquitylation to immunity and human disease. *Nature Reviews Immunology 2012 12:11*. 2012;12(11):774-785. doi:10.1038/nri3313

82. Malynn BA, Ma A. A20: A multifunctional tool for regulating immunity and preventing disease. *Cell Immunol*. 2019;340:103914. doi:10.1016/J.CELLIMM.2019.04.002

83. Shi Y, Wang X, Wang J, Wang X, Zhou H, Zhang L. The dual roles of A20 in cancer. *Cancer Lett*. 2021;511:26-35. doi:10.1016/J.CANLET.2021.04.017

84. Liao Y, Cao L, Wang F, Pang R. miR-605-5p promotes invasion and proliferation by targeting TNFAIP3 in non–small-cell lung cancer. *J Cell Biochem*. 2020;121(1):779-787. doi:10.1002/JCB.29323

85. Langsch S, Baumgartner U, Haemmig S, et al. miR-29b mediates NF-κkB signaling in KRAS-Induced non-small cell lung cancers. *Cancer Res*. 2016;76(14):4160-4169. doi:10.1158/0008-5472.CAN-15-2580

86. Breitenecker K, Homolya M, Luca AC, et al. Down-regulation of A20 promotes immune escape of lung adenocarcinomas. *Sci Transl Med*. 2021;13(601). doi:10.1126/SCITRANSLMED.ABC3911

87. Higgs BW, Morehouse CA, Streicher K, et al. Interferon gamma messenger RNA Signature in tumor biopsies predicts outcomes in patients with non–small cell lung carcinoma or urothelial cancer treated with durvalumab. *Clinical Cancer Research*. 2018;24(16):3857-3866. doi:10.1158/1078-0432.CCR-17-3451

88. Dong ZY, Zhang JT, Liu SY, et al. EGFR mutation correlates with uninflamed phenotype and weak immunogenicity, causing impaired response to PD-1 blockade in non-small cell lung cancer. *Oncoimmunology*. 2017;6(11). doi:10.1080/2162402X.2017.1356145

89. Xiao G, Li L, Tanzhu G, et al. Heterogeneity of tumor immune microenvironment of EGFR/ALK-positive tumors versus EGFR/ALK-negative tumors in resected brain metastases from lung adenocarcinoma. *J Immunother Cancer*. 2023;11(3):e006243. doi:10.1136/JITC-2022-006243

90. Liu L, Wang C, Li S, Bai H, Wang J. Tumor immune microenvironment in epidermal growth factor receptor-mutated non-small cell lung cancer before and after epidermal growth factor receptor tyrosine kinase inhibitor treatment: a narrative review. *Transl Lung Cancer Res*. 2021;10(9):3823. doi:10.21037/TLCR-21-572

91. Zhao Y, Tang G, Li J, Bian X, Zhou X, Feng J. Integrative transcriptome analysis reveals the molecular events underlying impaired T-cell responses in EGFR-mutant lung cancer. *Scientific Reports 2024 14:1*. 2024;14(1):1-20. doi:10.1038/S41598-024-69020-3

92. To KKW, Fong W, Cho WCS. Immunotherapy in Treating EGFR-Mutant Lung Cancer: Current Challenges and New Strategies. *Front Oncol*. 2021;11:635007. doi:10.3389/FONC.2021.635007

93. Van De Haar J, Mankor JM, Hummelink K, et al. Combining Genomic Biomarkers to Guide Immunotherapy in Non–Small Cell Lung Cancer. *Clinical Cancer Research*. 2024;30(7):1307. doi:10.1158/1078-0432.CCR-23-4027

94. Dai Y, Tian X, Ye X, Gong Y, Xu L, Jiao L. Role of the TME in immune checkpoint blockade resistance of non-small cell lung cancer. *Cancer Drug Resist 2024;7:52*. 2024;7(0):N/A-N/A. doi:10.20517/CDR.2024.166

95. McFadden DG, Politi K, Bhutkar A, et al. Mutational landscape of EGFR-, MYC-, and Kras-driven genetically engineered mouse models of lung adenocarcinoma. *Proc Natl Acad Sci U S A*. 2016;113(42):E6409-E6417. doi:10.1073/PNAS.1613601113

96. Hao Z, Rajewsky K. Homeostasis of peripheral B cells in the absence of B cell influx from the bone marrow. *Journal of Experimental Medicine*. 2001;194(8):1151-1163. doi:10.1084/JEM.194.8.1151,

97. DuPage M, Dooley AL, Jacks T. Conditional mouse lung cancer models using adenoviral or lentiviral delivery of Cre recombinase. *Nature Protocols 2009 4:7*. 2009;4(7):1064-1072. doi:10.1038/nprot.2009.95

98. Subramanian A, Tamayo P, Mootha VK, et al. Gene set enrichment analysis: A knowledge-based approach for interpreting genome-wide expression profiles. *Proc Natl Acad Sci U S A*. 2005;102(43):15545-15550. doi:10.1073/PNAS.0506580102

99. Mootha VK, Lindgren CM, Eriksson KF, et al. PGC-1α-responsive genes involved in oxidative phosphorylation are coordinately downregulated in human diabetes. *Nat Genet*. 2003;34(3):267-273. doi:10.1038/NG1180

100. Love MI, Huber W, Anders S. Moderated estimation of fold change and dispersion for RNA-seq data with DESeq2. *Genome Biol*. 2014;15(12):1-21. doi:10.1186/S13059-014-0550-8

101. Liu S, Liang J, Liu Z, et al. The Role of CD276 in Cancers. *Front Oncol*. 2021;11:654684. doi:10.3389/FONC.2021.654684

102. Kythreotou A, Siddique A, Mauri FA, Bower M, Pinato DJ. PD-L1. *J Clin Pathol*. 2018;71(3):189-194. doi:10.1136/JCLINPATH-2017-204853

103. Klebanoff CA, Finkelstein SE, Surman DR, et al. IL-15 enhances the in vivo antitumor activity of tumor-reactive CD8 + T Cells. *Proc Natl Acad Sci U S A*. 2004;101(7):1969-1974. doi:10.1073/PNAS.0307298101

104. Ali MS, Sayeski PP, Bernstein KE. Jak2 acts as both a STAT1 kinase and as a molecular bridge linking STAT1 to the angiotensin II AT1 receptor. *J Biol Chem*. 2000;275(20):15586-15593. doi:10.1074/jbc.M908931199

105. Ritz U, Seliger B. The Transporter Associated With Antigen Processing (TAP): Structural Integrity, Expression, Function, and Its Clinical Relevance. *Molecular Medicine*. 2001;7(3):149-158. doi:10.1007/BF03401948

106. Bournazou E, Bromberg J. Targeting the tumor microenvironment. *JAKSTAT*. 2013;2(2):e23828. doi:10.4161/JKST.23828

107. Luo M, Wang X, Wu S, et al. A20 promotes colorectal cancer immune evasion by upregulating STC1 expression to block “eat-me” signal. *Signal Transduct Target Ther*. 2023;8(1):1-13. doi:10.1038/S41392-023-01545-X

108. Guo W, Ma J, Guo S, et al. A20 regulates the therapeutic effect of anti-PD-1 immunotherapy in melanoma. *J Immunother Cancer*. 2020;8(2):e001866. doi:10.1136/JITC-2020-001866

109. Seungyeon Lim. *The Role of A20 as an Oncogene in Immunogenic EGFR-Driven Lung Adenocarcinoma*. Master Thesis. Medical University of Vienna; 2024.

110. Avalle L, Pensa S, Regis G, Novelli F, Poli V. STAT1 and STAT3 in tumorigenesis. *JAKSTAT*. 2012;1(2):65-72. doi:10.4161/JKST.20045

111. Mikucki ME, Fisher DT, Matsuzaki J, et al. Non-redundant requirement for CXCR3 signalling during tumoricidal T-cell trafficking across tumour vascular checkpoints. *Nature Communications 2015 6:1*. 2015;6(1):1-14. doi:10.1038/ncomms8458

112. Xia JB, Liu GH, Chen ZY, et al. Hypoxia/ischemia promotes CXCL10 expression in cardiac microvascular endothelial cells by NFkB activation. *Cytokine*. 2016;81:63-70. doi:10.1016/J.CYTO.2016.02.007

113. Yeruva S, Ramadori G, Raddatz D. NF-κB-dependent synergistic regulation of CXCL10 gene expression by IL-1β and IFN-γ in human intestinal epithelial cell lines. *Int J Colorectal Dis*. 2008;23(3):305-317. doi:10.1007/S00384-007-0396-6

114. Méndez-Samperio P, Pérez A, Rivera L. Mycobacterium bovis Bacillus Calmette-Guérin (BCG)-induced activation of PI3K/Akt and NF-kB signaling pathways regulates expression of CXCL10 in epithelial cells. *Cell Immunol*. 2009;256(1-2):12-18. doi:10.1016/J.CELLIMM.2008.12.002

115. Qian WJ, Yan JS, Gang XY, et al. Intercellular adhesion molecule-1 (ICAM-1): From molecular functions to clinical applications in cancer investigation. *Biochimica et Biophysica Acta (BBA) - Reviews on Cancer*. 2024;1879(6):189187. doi:10.1016/J.BBCAN.2024.189187

116. Riegler J, Gill H, Ogasawara A, et al. VCAM-1 Density and Tumor Perfusion Predict T-cell Infiltration and Treatment Response in Preclinical Models. *Neoplasia*. 2019;21(10):1036-1050. doi:10.1016/J.NEO.2019.08.003

117. Wu TC. The Role of Vascular Cell Adhesion Molecule-1 in Tumor Immune Evasion. *Cancer Res*. 2007;67(13):6003. doi:10.1158/0008-5472.CAN-07-1543

118. Mlecnik B, Tosolini M, Charoentong P, et al. Biomolecular Network Reconstruction Identifies T-Cell Homing Factors Associated With Survival in Colorectal Cancer. *Gastroenterology*. 2010;138(4):1429-1440. doi:10.1053/J.GASTRO.2009.10.057

119. Wu X, Giobbie-Hurder A, Liao X, et al. VEGF neutralization plus CTLA-4 blockade alters soluble and cellular factors associated with enhancing lymphocyte infiltration and humoral recognition in Melanoma. *Cancer Immunol Res*. 2016;4(10):858-868. doi:10.1158/2326-6066.CIR-16-0084

120. Seaman S, Zhu Z, Saha S, et al. Eradication of Tumors through Simultaneous Ablation of CD276/B7-H3-Positive Tumor Cells and Tumor Vasculature. *Cancer Cell*. 2017;31(4):501-515.e8. doi:10.1016/J.CCELL.2017.03.005

121. Khan S, Cameron S, Blaschke M, et al. Differential gene expression of chemokines in KRAS and BRAF mutated colorectal cell lines: Role of cytokines. *World Journal of Gastroenterology : WJG*. 2014;20(11):2979. doi:10.3748/WJG.V20.I11.2979

122. McGuire CK, Meehan AS, Couser E, et al. Transcriptional repression by HDAC3 mediates T cell exclusion from Kras mutant lung tumors. *Proc Natl Acad Sci U S A*. 2024;121(42):e2317694121. doi:10.1073/PNAS.2317694121

123. Harjunpää H, Asens ML, Guenther C, Fagerholm SC. Cell adhesion molecules and their roles and regulation in the immune and tumor microenvironment. *Front Immunol*. 2019;10(MAY):448153. doi:10.3389/FIMMU.2019.01078

124. Zhou WT, Jin WL. B7-H3/CD276: An Emerging Cancer Immunotherapy. *Front Immunol*. 2021;12:701006. doi:10.3389/FIMMU.2021.701006

125. Cha JH, Chan LC, Li CW, Hsu JL, Hung MC. Mechanisms Controlling PD-L1 Expression in Cancer. *Mol Cell*. 2019;76(3):359-370. doi:10.1016/J.MOLCEL.2019.09.030

126. Wang W, Lopez McDonald MC, Kim C, et al. The complementary roles of STAT3 and STAT1 in cancer biology: insights into tumor pathogenesis and therapeutic strategies. *Front Immunol*. 2023;14:1265818. doi:10.3389/FIMMU.2023.1265818

127. Berkley K, Zalejski J, Sharma N, Sharma A. Journey of PROTAC: From Bench to Clinical Trial and Beyond. *Biochemistry*. 2025;64:580. doi:10.1021/ACS.BIOCHEM.4C00577

128. Isazadeh H, Oruji F, Shabani S, et al. Advances in siRNA delivery approaches in cancer therapy: challenges and opportunities. *Molecular Biology Reports 2023 50:11*. 2023;50(11):9529-9543. doi:10.1007/S11033-023-08749-Y